

Flexible Basis Representations for Modeling Large Non-Gaussian Spatial Data

Remy MacDonald and Benjamin Seiyon Lee
Department of Statistics, George Mason University

Abstract

Nonstationary and non-Gaussian spatial data are common in various fields, including ecology (e.g., counts of animal species), epidemiology (e.g., disease incidence counts in susceptible regions), and environmental science (e.g., remotely-sensed satellite imagery). Due to modern data collection methods, the size of these datasets have grown considerably. Spatial generalized linear mixed models (SGLMMs) are a flexible class of models used to model nonstationary and non-Gaussian datasets. Despite their utility, SGLMMs can be computationally prohibitive for even moderately large datasets (e.g., 5,000 to 100,000 observed locations). To circumvent this issue, past studies have embedded nested radial basis functions into the SGLMM. However, two crucial specifications (knot placement and bandwidth parameters), which directly affect model performance, are typically fixed prior to model-fitting. We propose a novel approach to model large nonstationary and non-Gaussian spatial datasets using adaptive radial basis functions. Our approach: (1) partitions the spatial domain into subregions; (2) employs reversible-jump Markov chain Monte Carlo (RJMCMC) to infer the number and location of the knots within each partition; and (3) models the latent spatial surface using partition-varying and adaptive basis functions. Through an extensive simulation study, we show that our approach provides more accurate predictions than competing methods while preserving computational efficiency. We demonstrate our approach on two environmental datasets - incidences of plant species and counts of bird species in the United States.

Keywords: Bayesian Hierarchical Spatial Models; Non-Gaussian Spatial Models; Nonstationary Spatial Processes; Reversible-Jump MCMC; Spatial Basis Functions; Spatial Partitioning; Spatial Statistics.

1 Introduction

Discrete non-Gaussian spatial datasets (counts, binary responses, extreme values) are prevalent across a number of disciplines, such as ecology (Guan and Haran, 2018), public health (Ejigu et al., 2020), and atmospheric sciences (Sengupta et al., 2016; Heaton, Christensen and Terres, 2017). Modeling such datasets can be important for scientific applications, particularly in making predictions at unobserved locations and assessing prediction uncertainty. However, traditional regression models, which assume independent and identically distributed errors, may be inappropriate for these data (Schabenberger and Gotway, 2005; Banerjee, Carlin and Gelfand, 2003; Cressie, 1993) as they neglect spatial autocorrelation.

Spatial generalized linear mixed models (SGLMMs) (Diggle, Tawn and Moyeed, 1998; Haran, 2011) are a flexible class of spatial models that extend to non-Gaussian observations. Within SGLMMs, the spatial dependence is captured via location-specific random effects that are modeled as a latent Gaussian process (GP). Despite their flexibility, standard implementation of SGLMMs incurs a computational cost that is cubic in the data size, which can be computationally prohibitive for modeling modern spatial datasets. Additionally, the high-dimensional spatial random effects are typically highly correlated; thereby resulting in slow mixing Markov chain Monte Carlo (MCMC) algorithms (Haran, Hodges and Carlin, 2003).

Computationally-efficient approaches have been developed to reduce the dimensionality of the spatial random effects, speed up large matrix operations, or both. These include low-

rank approximations and basis representations (Cressie and Johannesson, 2006; Banerjee et al., 2008; Finley et al., 2009), sparse covariance and precision matrices (Furrer, Genton and Nychka, 2006; Datta et al., 2016; Vecchia, 1988; Zilber and Katzfuss, 2021), spatial partial differential equations (Lindgren, Rue and Lindström, 2011), spatial partitioning (Lee and Park, 2023; Heaton, Christensen and Terres, 2017), and more. Two prominent examples include nearest-neighbor Gaussian processes (NNGP) (Datta et al., 2016) and Integrated nested Laplace approximations (INLA) (Lindgren and Rue, 2015). NNGP approximates the GP using a sparse Cholesky factorization of the specified precision matrix. Sparsity is induced by directed acyclical graphs that connect neighboring locations. While NNGP preserves the flexibility and interpretability of GP models, the SGLMM framework requires the inference of all n spatial random effects. This can be prohibitive for large discrete non-Gaussian spatial datasets. Moreover, the spNNGP (Finley et al., 2009) package currently accommodates binary and Gaussian spatial data only; hence, it cannot directly model count observations (Dovers et al., 2023). INLA employs stochastic partial differential equations to provide fast and accurate numerical approximations of posterior distributions. INLA provides approximations of the marginal posterior distribution, rather than the joint distribution; hence, it may potentially underestimate the uncertainty in estimation and predictions (Ferkingstad and Rue, 2015).

In this manuscript, we focus on basis representation approaches which approximate the latent spatial process using a linear combination of spatial radial basis functions (e.g., bisquare, Wendland basis, and thin-plate-splines) (Zammit-Mangion and Cressie, 2018; Sengupta and Cressie, 2013; Katzfuss, 2017; Cressie and Johannesson, 2008; Lee and Park,

2023). For a comprehensive review of basis functions models in spatial statistics, please see Cressie, Sainsbury-Dale and Zammit-Mangion (2022). Two key components of radial basis functions are the knots (centers of the basis functions) and the associated bandwidth (or smoothing) parameters. The bandwidth defines the “spread” of the radial basis function and also tunes the tradeoff between the goodness-of-fit and the roughness of the resulting basis approximation (Kato and Shiohama, 2009). Poorly specified knots and bandwidths can result in inaccurate representations of the latent spatial surface (Sheather and Jones, 1991). Since specifying these parameters can be challenging, past studies (Cressie and Johannesson, 2008; Katzfuss and Cressie, 2011, 2012) have typically fixed them prior to model fitting. As a result, the spatial basis functions are constructed without any feedback or influence from the observed data.

To address these challenges, we propose a computationally efficient, yet flexible approach for modeling nonstationary non-Gaussian spatial data. Our method addresses the two limitations (knot placement and bandwidth specification) by allowing the spatial radial basis functions to adapt to the observations. Our method partitions the spatial domain into disjoint subregions and allows the bandwidths to vary across each subregion. For each partition, we employ a reversible jump Markov chain Monte Carlo (RJMCMC) algorithm (Green, 1995) to infer the number and placement of knots. The proposed approach allows for more flexibility than using fixed basis functions and scales well to large datasets.

Previous studies have focused on either adaptive knot selection (Billier, 2000; Denis, M and Molinari, N., 2010; Katzfuss, 2013) or adaptive bandwidth selection (Politis, 2003; Brockmann, Gasser, and Herrmann, 1993). To the best of our knowledge, our study is

the first to consider both adaptive bandwidth and adaptive knot selection simultaneously, especially within spatial models. While adaptive knot selection and bandwidth specification have been applied in splines and kernel regression, their use in spatial statistics remains limited. Additionally, our method differs from existing approaches by allowing partition-specific basis functions instead of assuming globally defined bases.

The outline of the remainder of the paper is as follows. In Section 2, we introduce SGLMMs and basis-expansion SGLMMs and discuss important modeling and computational challenges. In Section 3, we propose our approach (Adapt-BaSeS) and provide implementation details. We demonstrate our approach via a simulation study in Section 4 and real-world applications in Section 5. Concluding remarks and directions for future research are provided in Section 6.

2 Spatial Generalized Linear Mixed Models

SGLMMs (Diggle, Tawn and Moyeed, 1998) are a class of flexible models for modeling spatially-dependent non-Gaussian data. These models are a special case of generalized linear mixed models, where the random effects exhibit spatial correlation. Conditioned on the random effects, the observations are assumed to be independent and follow a location-specific probability distribution. SGLMMs have been used extensively in the literature to model non-Gaussian spatially-correlated data (Hughes and Haran, 2013; Zilber and Katzfuss, 2021; Zhang, 2002).

In the Bayesian framework, SGLMMs are part of the broader class of Bayesian hierarchical spatial models (HSM) (Wikle, Berliner, and Cressie, 1998). HSMs are comprised

of three layers or models: data, process, and parameters. The data model layer contains the probability distribution of the observed data (e.g., Gaussian, Bernoulli, multinomial) conditioned on the latent spatial Gaussian random fields and data model parameters. The process model layer includes conditional distributions for the Gaussian spatial process(es) conditioned on the process model parameters or other underlying processes. Note that the process models can be as simple (single latent process) or robust (multiple interconnected spatial random processes) as needed. Bayesian hierarchical models are applicable for modeling complex spatial processes where: (1) the spatial dependence is driven by a complex latent spatial random process; and (2) the practitioner has prior knowledge of the unknowns (e.g., model parameters and spatial processes).

Let $\{z(\mathbf{s}) : \mathbf{s} \in \mathcal{D}\}$ denote the non-Gaussian observations on the spatial domain $\mathcal{D} \subset \mathbb{R}^d$, $d \in \mathbb{N}$. At n locations, we have observations $\mathbf{z} = (z(\mathbf{s}_1), \dots, z(\mathbf{s}_n))^\top$, where $z(\cdot) \sim F(\cdot)$ for some distribution F . The conditional mean is modeled as $g(\mathbb{E}[z(\mathbf{s}_i)]) := \eta(\mathbf{s}_i)$ for $i = 1, \dots, n$, where $g(\cdot)$ is a link function and $\eta(\cdot)$ is the linear predictor. For location \mathbf{s}_i , the linear predictor is defined as,

$$\eta(\mathbf{s}_i) := \mathbf{x}(\mathbf{s}_i)^\top \boldsymbol{\beta} + w(\mathbf{s}_i),$$

where $\mathbf{x}(\mathbf{s}_i)$ is a vector of covariates with regression coefficients $\boldsymbol{\beta}$, and $w(\mathbf{s}_i)$ represents the spatially-correlated random effect, often modeled as a zero-mean GP $w(\cdot) \sim \mathcal{GP}(\mathbf{0}, K)$, where K is a covariance function with marginal variance σ^2 and a correlation function C , i.e., $K(\mathbf{s}_1, \mathbf{s}_2) = \sigma^2 C(\mathbf{s}_1, \mathbf{s}_2)$, $\mathbf{s}_1, \mathbf{s}_2 \in \mathcal{D}$. The correlation function $C : (\mathcal{D} \times \mathcal{D}) \rightarrow [-1, 1]$ is assumed to be known up to some parameters $\boldsymbol{\theta}$. A commonly used class of covariance functions, which assumes stationarity and isotropy, is the Matérn class (Williams and

Rasmussen, 2006), defined as,

$$\mathcal{M}_\nu(h) = \frac{2^{1-\nu}}{\Gamma(\nu)} \left(\sqrt{2\nu} \frac{d}{\rho} \right)^\nu \mathcal{K}_\nu \left(\sqrt{2\nu} \frac{d}{\rho} \right), \quad \nu, \rho > 0,$$

where $d = \|\mathbf{s}_i - \mathbf{s}_j\|$ denotes the Euclidean distance between pairs of locations, ρ is the spatial range parameter, ν is the smoothness parameter, $\Gamma(\cdot)$ is the gamma function, and $\mathcal{K}_\nu(\cdot)$ is the modified Bessel function of the second kind of order $\nu > 0$.

For a finite vector of locations $\mathcal{S} = (\mathbf{s}_1, \dots, \mathbf{s}_n)$, the spatial random effects $\mathbf{w} = (w(\mathbf{s}_1), \dots, w(\mathbf{s}_n))^\top$ follows a multivariate normal distribution $\mathbf{w} \mid \sigma^2, \boldsymbol{\theta} \sim \mathcal{N}(\mathbf{0}, \mathbf{K})$, where \mathbf{K} is an $n \times n$ covariance matrix whose entries are $K(\mathbf{s}_i, \mathbf{s}_j)$. Let $\boldsymbol{\eta} := (\eta(\mathbf{s}_1), \dots, \eta(\mathbf{s}_n))^\top$ denote the vector of transformed site-specific conditional means, such that the data model is given by $g(\mathbb{E}[\mathbf{z} \mid \boldsymbol{\beta}, \mathbf{w}]) := \boldsymbol{\eta} = \mathbf{X}\boldsymbol{\beta} + \mathbf{w}$ for some link function $g(\cdot)$. Here, each observation $z(\mathbf{s}_i)$ is assumed to be conditionally independent given $\eta(\mathbf{s}_i)$. Let $\mathbf{X} = [\mathbf{x}(\mathbf{s}_1), \dots, \mathbf{x}(\mathbf{s}_n)]^\top$ denote the covariate matrix. Then under the Bayesian hierarchical framework, SGLMMs are structured as follows:

$$\begin{aligned} \text{Data Model:} \quad & z(\mathbf{s}_i) \mid \eta(\mathbf{s}_i) \stackrel{\text{indpt}}{\sim} F(\eta(\mathbf{s}_i)) \\ & g(\mathbb{E}[\mathbf{z} \mid \boldsymbol{\beta}, \mathbf{w}]) := \boldsymbol{\eta} = \mathbf{X}\boldsymbol{\beta} + \mathbf{w} \\ \text{Process Model:} \quad & \mathbf{w} \mid \sigma^2, \boldsymbol{\theta} \sim \mathcal{N}(\mathbf{0}, \mathbf{K}) \\ \text{Parameter Model:} \quad & \sigma^2 \sim p(\sigma^2), \boldsymbol{\theta} \sim p(\boldsymbol{\theta}), \end{aligned} \tag{1}$$

with prior distributions $p(\sigma^2)$ and $p(\boldsymbol{\theta})$ specified by the practitioner.

Despite their flexibility, SGLMMs are subject to a myriad of limitations. In many cases, SGLMMs assume a second-order stationary and isotropic GP for the spatial random effects \mathbf{w} , where the covariance function depends solely on pairwise Euclidean distances. This assumption can be overly restrictive or unrealistic (Risser, 2016), especially for large

and heterogeneous spatial domains (Katzfuss, 2013). Furthermore, evaluating the density $\mathbf{w} \sim \mathcal{N}(\mathbf{0}, \mathbf{K})$ in SGLMMs requires $\mathcal{O}(n^3)$ operations and $\mathcal{O}(n^2)$ memory, which can be computationally prohibitive for large datasets. SGLMMs are often overparameterized, since all n highly-correlated random effects must be inferred. This can result in slow-mixing Markov chains in the MCMC algorithm (Haran, 2011).

2.1 Basis Function Representations

As discussed in the introduction, to alleviate the inferential and computational concerns of parameterizing all n highly-correlated random effects, the spatial random effects can be modeled as a low-rank (dimension-reduced) process using a basis function expansion. Basis representation approaches have been widely used for modeling complex spatial processes due to their flexibility and computational efficiency (Cressie and Wikle, 2011; Cressie, Sainsbury-Dale and Zammit-Mangion, 2022; Bradley, Cressie and Shi, 2011). These approaches represent the spatial process $w(\cdot)$ as a linear combination of m basis functions $\Phi(\mathbf{s}) = (\Phi_1(\mathbf{s}), \dots, \Phi_m(\mathbf{s}))^\top$ with corresponding basis coefficients $\boldsymbol{\delta} = (\delta_1, \dots, \delta_m)^\top$ such that,

$$w(\mathbf{s}) \approx \sum_{i=1}^m \Phi_i(\mathbf{s})\delta_i = \Phi(\mathbf{s})^\top \boldsymbol{\delta}, \quad \mathbf{s} \in \mathcal{D}, \quad (2)$$

where $\boldsymbol{\delta} \mid \boldsymbol{\Sigma}_\delta \sim \mathcal{N}_m(\mathbf{0}, \boldsymbol{\Sigma}_\delta)$. To reduce the dimension (or rank) and alleviate computational costs, we retain only the first $m \ll n$ basis functions. Let $\mathbf{\Phi}$ be an $n \times m$ matrix with columns indicating the basis functions and rows indicating the locations. Then by construction of (2), the approximated covariance matrix of \mathbf{w} is $\mathbf{\Phi}\boldsymbol{\Sigma}_\delta\mathbf{\Phi}^\top$. This does not solely depend on the distance between locations and is hence nonstationary. Furthermore, evaluating the

density $\boldsymbol{\delta} \mid \boldsymbol{\Sigma}_{\boldsymbol{\delta}} \sim \mathcal{N}_m(\mathbf{0}, \boldsymbol{\Sigma}_{\boldsymbol{\delta}})$ only involves matrix operations on matrices of size $m \times m$, which requires $\mathcal{O}(m^3)$ operations and $\mathcal{O}(m^2)$ storage.

Different types of basis functions have been used, including radial basis functions, such as multi-resolution basis functions (Sengupta et al., 2016; Cressie and Johannesson, 2008; Katzfuss and Cressie, 2011, 2012), Fourier basis functions (Xu, Wikle and Fox, 2005), eigenfunctions (Holland et al., 1999), and the predictive-process approach (Banerjee et al., 2008). Multi-resolution basis function approaches employ multiple layers of nested basis functions with varying resolutions to capture spatial structures from very fine to very large scale. For example, Sengupta et al. (2016) utilize a “quad-tree” structure comprised of low- and high-resolution bisquare basis functions. Royle and Wikle (2005) use Fourier basis functions to represent the spatial variability, a particularly useful method when working periodic or cyclical patterns in spatial data. When replicated spatial data are available, the eigenfunction approach employs eigenvectors of the dataset’s empirical covariance matrix (Higdon et al., 2008; Cressie and Wikle, 2015; Mak et al., 2018), and the eigenvector basis functions capture the major patterns of spatial variation. When no replicates are available, a related approach extracts the m -leading eigenvectors of a proposed parametric covariance matrix (e.g., Matérn class) (Guan and Haran, 2018; Christensen, Roberts, and Sköld, 2006) that is dependent on pointwise distances. The covariance parameters can then be inferred within the modeling framework. The predictive-process approach considers both $\Phi(\cdot)$ and $\boldsymbol{\Sigma}_w$ to be parameterized (e.g., Matérn class) according to a lower-dimensional “parent process.” Given the “parent process” $w(\cdot)$, the predictive process is defined as, $w^*(\cdot) = \mathbb{E}(w(\cdot) \mid w(\mathbf{u}_1), \dots, w(\mathbf{u}_m))$, where $\mathcal{K} = \{\mathbf{u}_1, \dots, \mathbf{u}_m\}$ is a set of knots.

In this manuscript, we focus on radial basis functions (e.g. Gaussian, bisquare, thin-plate-splines), which are usually parameterized by knots and bandwidth parameters. Despite their flexibility and low costs, radial basis functions require the user to pre-specify the: (1) number of knots; (2) knot locations; and (3) bandwidth parameters. For example, Sengupta et al. (2016) fix the bandwidths and knots associated with each resolution of nested layers of bisquare basis functions. Similarly, Nychka et al. (2015) employ fixed compactly supported radial basis functions to capture multiple scales of spatial dependency. This pre-specification can potentially constrain the hierarchical spatial model to a fixed set of basis functions without any feedback or influence from the observed data. Given the challenge of appropriately specifying the number and placement of knots in spatial data, it is crucial to employ adaptive methods for knot selection.

3 Adapt-BaSeS: Adaptive Basis Selection and Specification

Our proposed method, Adaptive Basis Selection and Specification (Adapt-BaSeS), is a flexible yet computationally efficient method for modeling nonstationary and non-Gaussian spatial data. The utility of Adapt-BaSeS comes from the adaptive tuning of radial basis functions, specifically the number and placement of knots as well as the bandwidths. Let $\mathcal{K} = (\mathbf{u}_1, \dots, \mathbf{u}_m)$ be a vector of m knots over the spatial domain \mathcal{D} and let $\epsilon > 0$ be the bandwidth parameter. Then the Gaussian radial basis function corresponding to knot \mathbf{u}_i

is defined as:

$$\Phi_i(\mathbf{s}) = \exp(-(\epsilon\|\mathbf{s} - \mathbf{u}_i\|^2)), \quad (3)$$

where $\|\cdot\|$ denotes the Euclidean distance between the points \mathbf{s} and \mathbf{u}_i . The choice of ϵ is crucial, as large values can lead to overfitting (Chaudhuri et al., 2017) and sharp localized peaks, while small values can oversmooth the latent spatial surface. Improper specification of the bandwidth parameters can lead to inaccurate predictions and improper approximations of the latent spatial surfaces (Sheather and Jones, 1991; Damodaran, 2018).

Adapt-BaSeS addresses these challenges by embedding an adaptive basis selection and specification mechanism within the SGLMM framework. First, we partition the spatial domain into disjoint subregions using an agglomerative clustering algorithm (Heaton, Christensen and Terres, 2017). Next, we fit a hierarchical spatial model with partition-specific and adaptive radial basis functions to model the observed data. Our algorithmic approach employs a RJMCMC algorithm (Green, 1995) to select key features of the radial basis functions (e.g., knot locations, total number of bases, and bandwidths) with clear feedback from the data. To the best of our knowledge, this study is the first to allow for both adaptive bandwidths and knots for basis-representation SGLMMs.

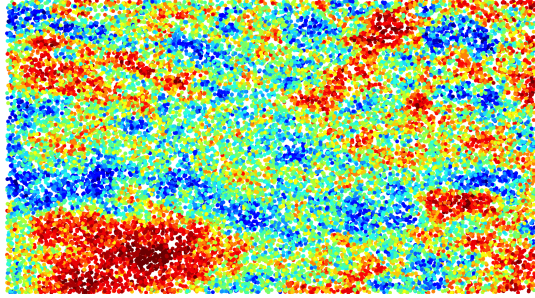
3.1 Spatial Partitioning

Let $\mathbf{z} = (z(\mathbf{s}_1), \dots, z(\mathbf{s}_n))^\top$ denote observations at locations $\mathbf{s}_i \in \mathcal{D}$. We use an agglomerative clustering approach (Heaton, Christensen and Terres, 2017) to partition the spatial locations into K disjoint subregions $\{\mathcal{D}_k\}_{k=1}^K$ such that $\bigcup_{k=1}^K \mathcal{D}_k = \mathcal{D}$ and $\mathcal{D}_i \cap \mathcal{D}_j = \emptyset$ for

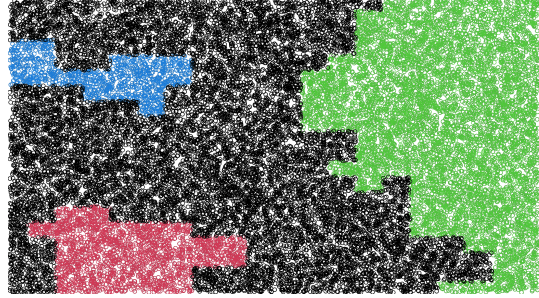
all $i \neq j$. To accomplish this, the dissimilarity between $z(\mathbf{s}_i)$ and $z(\mathbf{s}_j)$ is:

$$d_{ij} = d(z(\mathbf{s}_i), z(\mathbf{s}_j)) = \frac{|z(\mathbf{s}_i) - z(\mathbf{s}_j)|}{\|\mathbf{s}_i - \mathbf{s}_j\|}.$$

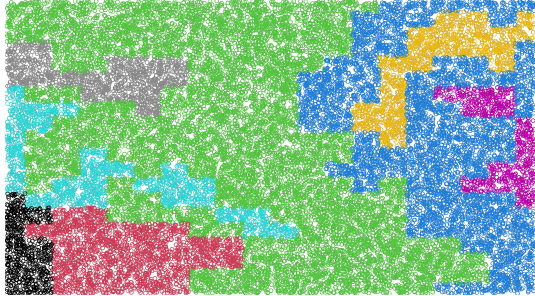
The dissimilarity metric d_{ij} is based on spatial finite differences, which estimate the directional derivative (Banerjee, Gelfand, and Sirmans, 2003). This metric measures dissimilarity by considering how the spatial surface changes between two locations. When the surface changes rapidly in the direction from \mathbf{s}_i to \mathbf{s}_j , the dissimilarity is large, indicating that $z(\mathbf{s}_i)$ and $z(\mathbf{s}_j)$ should be assigned to different clusters (Heaton, Christensen and Terres, 2017). An agglomerative clustering approach is then used, where $K = n$ clusters are initialized such that each observation starts as its own cluster. Clusters are then linked together based on the smallest dissimilarity and spatial contiguity is enforced by only clustering Voronoi neighbors. This process is then repeated until the desired K partitions is reached. We then let $\mathbf{z}_k = \{z(\mathbf{s}_i) : \mathbf{s}_i \in \mathcal{D}_k \subset \mathcal{D}\}$ for $i = 1, \dots, n_k$ denote the n_k observations belonging to the k -th partition, such that $n = \sum_{k=1}^K n_k$. For additional details on the clustering algorithm, please refer to the supplement. Alternatively, dissimilarity can be defined using the residuals from a regression with non-spatial errors (Heaton, Christensen and Terres, 2017). In particular, the residuals are computed as $(z_i - \mathbb{E}[z_i | \mathbf{x}_i])$, where $\mathbb{E}[z_i | \mathbf{x}_i]$ comes from a generalized linear model. For count data (Poisson data model), $\mathbb{E}[z_i | \mathbf{x}_i]$ would be the expected intensity $\exp(\mathbf{x}_i^\top \hat{\boldsymbol{\beta}})$, and for binary data (Bernoulli data model), $\mathbb{E}[z_i | \mathbf{x}_i]$ would be the expected probability $1 / \exp(-\mathbf{x}_i^\top \hat{\boldsymbol{\beta}})$. For non-Gaussian data, we find that this alternative approach outperforms clustering based on the observations themselves. Figure 1 illustrates the spatial partitioning for one simulated dataset, with different colors representing disjoint partitions.



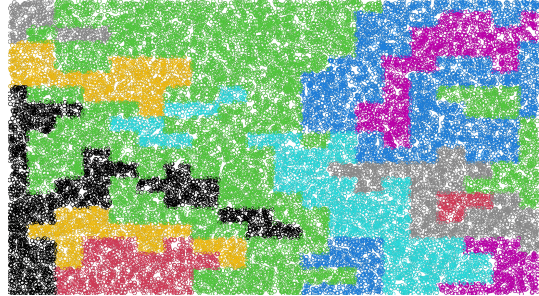
(a) Spatial Surface



(b) Partition of Spatial Domain ($K = 4$)



(c) Partition of Spatial Domain ($K = 8$)



(d) Partition of Spatial Domain ($K = 16$)

Figure 1: Illustration of spatial partitioning. (a) Spatial observations. (b) Observations partitioned into 4 subregions; different colors indicate disjoint partitions. (c) Case for 8 partitions. (d) Case for 16 partitions.

3.2 Bayesian Hierarchical Model

For partition $k = 1, \dots, K$, the conditional mean $\mathbb{E}[\mathbf{z}_k \mid \boldsymbol{\beta}_k, \boldsymbol{\delta}_k, \epsilon_k, \mathcal{K}_k, \boldsymbol{\gamma}]$ is modeled as,

$$g(\mathbb{E}[\mathbf{z}_k \mid \boldsymbol{\beta}_k, \boldsymbol{\delta}_k, \epsilon_k, \mathcal{K}_k, \boldsymbol{\gamma}]) := \boldsymbol{\eta}_k = \mathbf{X}_k \boldsymbol{\beta}_k + \boldsymbol{\Phi}_k(\epsilon_k, \mathcal{K}_k) \boldsymbol{\delta}_k + \mathbf{H}_k \boldsymbol{\gamma}, \quad (4)$$

where \mathbf{X}_k is an $n_k \times p$ covariate matrix with corresponding regression coefficients $\boldsymbol{\beta}_k = (\beta_{k1}, \dots, \beta_{kp})^\top$, $\mathcal{K}_k = (\mathbf{u}_{k,1}, \dots, \mathbf{u}_{k,r_k})$ is a vector of partition-specific knots, ϵ_k is a partition-specific bandwidth parameter, $\boldsymbol{\Phi}_k(\epsilon_k, \mathcal{K}_k)$ is an $n_k \times r_k$ adaptive radial basis function matrix with basis coefficients $\boldsymbol{\delta}_k = (\delta_{k1}, \dots, \delta_{kr_k})^\top$, and \mathbf{H}_k is a basis function matrix with global coefficients $\boldsymbol{\gamma} = (\gamma_1, \dots, \gamma_g)^\top$.

For the combined vector of observations $\mathbf{z} = (\mathbf{z}_1^\top, \dots, \mathbf{z}_K^\top)^\top$, (4) implies that,

$$g(\mathbb{E}[\mathbf{z} \mid \boldsymbol{\beta}, \boldsymbol{\delta}, \boldsymbol{\epsilon}, \mathcal{K}, \boldsymbol{\gamma}]) := \boldsymbol{\eta} = \mathbf{X}\boldsymbol{\beta} + \boldsymbol{\Phi}(\boldsymbol{\epsilon}, \mathcal{K})\boldsymbol{\delta} + \mathbf{H}\boldsymbol{\gamma},$$

where \mathbf{X} is a block-diagonal matrix with matrices \mathbf{X}_k on the main diagonal, $\boldsymbol{\beta} = (\boldsymbol{\beta}_1^\top, \dots, \boldsymbol{\beta}_K^\top)^\top$, $\boldsymbol{\epsilon} = (\epsilon_1, \dots, \epsilon_K)$, $\boldsymbol{\Phi}(\boldsymbol{\epsilon}, \mathcal{K})$ is a block-diagonal matrix with matrices $\boldsymbol{\Phi}_k(\epsilon_k, \mathcal{K}_k)$ on the main diagonal, $\boldsymbol{\delta} = (\boldsymbol{\delta}_1^\top, \dots, \boldsymbol{\delta}_K^\top)^\top$, and \mathbf{H} is an $n \times g$ matrix stacking the individual \mathbf{H}_k matrices. The parameter ϵ_k determines the smoothness of the basis functions associated with the k -th partition. By allowing ϵ_k to vary across partitions, our approach can capture the smooth and rough surfaces of the heterogeneous spatial domain.

Since the basis functions (3) are infinitely differentiable, it is possible that the surfaces resulting from the basis expansions will be infinitely smooth. However, we find that letting ϵ_k be sufficiently large obviates this challenge in practical applications. Additionally, there may be concern that if the number of partitions K is too small, the global and partitioned basis functions could be collinear due to their similar spatial scales. However, we have designed them to mitigate this issue. First, both types of basis functions have compact support. Second, the knots (basis centers) for the global and partitioned basis functions are unique and do not overlap. Third, the basis functions for the global and partitioned sets are from different classes. Specifically, we use bisquare basis functions for the global bases and Gaussian basis functions for the partitioned set. Fourth, since the partitioned basis functions are designed to capture finer-scale dependencies, we can limit the overlap by imposing constraints on the global basis functions' bandwidths. Similarly, we suggest practitioners use informative prior distributions for the partition-specific bandwidth parameters. Although we have made an effort to minimize collinearity issues, they may still

arise in certain applications. In such cases, the model may become non-identifiable, compromising the estimation of the corresponding basis coefficients. However, it's worth noting that while this may affect the individual estimates of the basis coefficients, the overall predictions (kriging) of the model would remain sound, even if the individual estimates are not precise (Baker et al., 2022).

In many applications, it may be desirable to have global regression coefficients such that $\boldsymbol{\beta} = \boldsymbol{\beta}_1 = \dots = \boldsymbol{\beta}_K$. In that setting, \mathbf{X} would be an $n \times p$ matrix stacking the \mathbf{X}_k matrices. Using Adapt-BaSeS, the hierarchical spatial model is:

$$\begin{aligned}
 \text{Data Model:} \quad & z(\mathbf{s}_i) \mid \eta(\mathbf{s}_i) \stackrel{\text{indpt}}{\sim} F(\eta(\mathbf{s}_i)) \\
 & g(\mathbb{E}[z \mid \boldsymbol{\beta}, \boldsymbol{\delta}, \boldsymbol{\epsilon}, \mathcal{K}, \boldsymbol{\gamma}]) := \boldsymbol{\eta} = \mathbf{X}\boldsymbol{\beta} + \boldsymbol{\Phi}(\boldsymbol{\epsilon}, \mathcal{K})\boldsymbol{\delta} + \mathbf{H}\boldsymbol{\gamma} \\
 \text{Process Model:} \quad & \boldsymbol{\delta}_k \mid \tau_k^2 \sim \mathcal{N}(\mathbf{0}, \tau_k^2 \mathcal{I}) \\
 & \boldsymbol{\gamma} \mid \rho^2 \sim \mathcal{N}(\mathbf{0}, \rho^2 \mathcal{I}) \\
 \text{Parameter Model:} \quad & \boldsymbol{\beta}_k \sim p(\boldsymbol{\beta}_k), \epsilon_k \sim p(\epsilon_k), \tau_k^2 \sim p(\tau_k^2), \\
 & \mathcal{K}_k \sim p(\mathcal{K}_k), \rho^2 \sim p(\rho^2),
 \end{aligned} \tag{5}$$

where \mathcal{I} denotes the identity matrix. We complete the hierarchical spatial model by specifying the prior distributions for the model parameters $\boldsymbol{\beta}_k$, ϵ_k , τ_k^2 , ρ^2 , and \mathcal{K}_k . We can reduce computational costs by limiting the number of basis functions r_k within each partition to be small and by specifying the covariance matrices $\boldsymbol{\Sigma}_{\boldsymbol{\delta}_k}$ and $\boldsymbol{\Sigma}_{\boldsymbol{\gamma}}$ to be diagonal (Lee and Park, 2023; Higdon, 1998; Lindgren, Rue and Lindström, 2011; Nychka et al., 2015). One can introduce a predefined covariance structure for the basis coefficients, such as employing an exponential covariance function (Heaton et al., 2019). However, this would result in additional computational overhead. Conditional on $\boldsymbol{\gamma}$, the parameters $\boldsymbol{\beta}_k$, \mathcal{K}_k , $\boldsymbol{\delta}_k$, ϵ_k , and

τ_k^2 can be estimated independently for each partition. Hence, the MCMC updates of these parameters can be done in parallel to facilitate computational efficiency.

We note that our approach assumes local nonstationarity because the partition-specific basis functions yield a nonstationary covariance structure. In addition, each partition has a different nonstationary covariance structure. This is in contrast to weighted-average methods approaches (Fuentes, 2001; Risser, M. D. and Calder, C. A., 2015; Kim, Mallick, and Holmes, 2005) which construct nonstationary spatial processes by smoothing locally stationary processes.

3.3 The Reversible-Jump MCMC Algorithm

We propose a RJMCMC algorithm (Algorithm 1) to select the number and placement of knots within each partition. For a given partition k , we take the number of knots r_k to be random, from some countable set $\mathcal{S}_k = \{0, \dots, R_k\}$, where R_k is the number of candidate knots in partition k . Let \mathcal{M}_{r_k} denote the model with exactly r_k knots and let $\mathcal{K}_k(r_k) = \{\mathbf{u}_{k,1}, \dots, \mathbf{u}_{k,r_k}\}$ denote the knots. We generate samples from the joint posterior of $(r_k, \mathcal{K}_k(r_k))$. To account for the varying dimensionality, we must develop appropriate reversible jump moves. For this problem, possible transitions are: (1) add a knot (birth step), (2) delete a knot (death step), and (3) move a knot. These independent move types are randomly chosen with probability b_{r_k} for the move r_k to $r_k + 1$ (birth step), d_{r_k} for the move r_k to $r_k - 1$ (death step), and η_{r_k} for the move step. These probabilities must satisfy $b_{r_k} + d_{r_k} + \eta_{r_k} = 1$. For this choice, we define $b_0 = d_{R_k} = 1$ and $b_{r_k} = d_{r_k} = \eta_{r_k} = 1/3$ otherwise.

3.3.1 Prior Specifications

We specify a truncated Poisson prior distribution for r_k , such that

$$p(r_k) \propto \frac{\lambda^{r_k} \exp(-\lambda)}{r_k!} \mathbb{1}_{\{0, \dots, R_k\}}(r_k).$$

The choice of λ is a compromise between model flexibility and model parsimony. A small value of λ reflects a strong incidence of smoothness whereas a large value may cause the model to fit the data too closely. The choice of λ will be discussed later.

For a given r_k , the knots are randomly selected with equal probability from a set of candidate knots $\mathcal{R}_k = \{\mathbf{u}_{k,1}, \dots, \mathbf{u}_{k,R_k}\}$, where $\mathbf{u}_{k,1}, \dots, \mathbf{u}_{k,R_k}$ are equally-spaced over the subregion \mathcal{D}_k . Given r_k , the prior distribution for $\mathcal{K}_k(r_k) = \{\mathbf{u}_{k,1}, \dots, \mathbf{u}_{k,r_k}\}$ is then given by

$$p(\mathcal{K}_k(r_k) \mid r_k) = \binom{R_k}{r_k}^{-1} = \frac{r_k!(R_k - r_k)!}{R_k!}.$$

A commonly used prior for regression coefficients of a generalized linear model is the multivariate normal distribution $\boldsymbol{\delta}_k \mid r_k \sim \mathcal{N}(\mathbf{0}, \boldsymbol{\Sigma}_{\boldsymbol{\delta}_k})$ (Gamerman, 1997). Following Biller (2000), we assume the basis coefficients $\boldsymbol{\delta}_k$ are uncorrelated, i.e., $\boldsymbol{\Sigma}_{\boldsymbol{\delta}_k} = \tau_k^2 \mathcal{I}$.

3.3.2 Algorithm

At each step of the RJMCMC algorithm, we propose one of three modifications to the current set of r_k knots for each partition k :

1. **Add a knot (birth step):** Draw a new knot \mathbf{u}_{k,r_k+1} uniformly with probability $1/(R_k - r_k)$ from the set of the $R_k - r_k$ vacant knots. Let $\mathcal{K}_k^* = \mathcal{K}_k \cup \{\mathbf{u}_{k,r_k+1}\}$ be the proposed set of knots, which now has size $r_k^* = r_k + 1$.

2. **Delete a knot (death step):** Select a knot $\mathbf{u}_{k,J}$ uniformly at random from one of the r_k current knots, so it is drawn with probability $1/r_k$. Then set $\mathcal{K}_k^* = \mathcal{K}_k \setminus \{\mathbf{u}_{k,J}\}$ and $r_k^* = r_k - 1$.
3. **Move a knot (move step):** Select a knot $\mathbf{u}_{k,J}$ uniformly at random to be deleted, and then select a new location \mathbf{u}_{k,r_k+1} from the vacant knots (i.e., where to move the old knot). This results in $\mathcal{K}_k^* = \{\mathbf{u}_{k,r_k+1}\} \cup \mathcal{K}_k \setminus \{\mathbf{u}_{k,J}\}$ and $r_k^* = r_k$.

Note that when we propose to add a knot \mathbf{u}_{k,r_k+1} , a corresponding basis coefficient δ_{k,r_k+1}^* will also need to be proposed. Similarly, if we propose to delete a knot $\mathbf{u}_{k,J}$, the current basis coefficient $\delta_{k,J}$ will be set to 0. If we propose to move a knot, we will propose changing the current basis coefficient from $\delta_{k,J}$ to δ_{k,r_k+1}^* . Complete details of the RJMCMC algorithm can be seen in Algorithm 1. Proposition 1 asserts that a sufficient choice for the acceptance probability is given by (6); hence fulfilling the detailed balance condition.

Proposition 1. *The detailed balance condition is satisfied by setting the acceptance probability to be $\min\{1, \alpha\}$, where*

$$\alpha = \frac{L(\mathbf{z}_k \mid \mathcal{K}_k^*, \boldsymbol{\delta}_k^*) \pi(\mathcal{K}_k^*, \boldsymbol{\delta}_k^*) Q(\mathcal{K}_k^*, \mathcal{K}_k)}{L(\mathbf{z}_k \mid \mathcal{K}_k, \boldsymbol{\delta}_k) \pi(\mathcal{K}_k, \boldsymbol{\delta}_k) Q(\mathcal{K}_k, \mathcal{K}_k^*)}, \quad (6)$$

and the proposal ratio is given by,

$$\frac{Q(\mathcal{K}_k^*, \mathcal{K}_k)}{Q(\mathcal{K}_k, \mathcal{K}_k^*)} = \begin{cases} \frac{R_k - r_k}{r_k + 1} \times \frac{1}{\mathcal{N}(\delta_{k,r_k+1}^*; 0, \sigma^2)}, & r_k^* = r_k + 1 \\ \frac{r_k}{R_k - r_k + 1} \times \mathcal{N}(\delta_{k,J}; 0, \sigma^2), & r_k^* = r_k - 1 \\ \frac{\mathcal{N}(\delta_{k,J}; 0, \sigma^2)}{\mathcal{N}(\delta_{k,r_k+1}^*; 0, \sigma^2)}, & r_k^* = r_k, \end{cases}$$

and the prior ratio is given by,

$$\frac{\pi(\mathcal{K}_k^*, \boldsymbol{\delta}_k^*)}{\pi(\mathcal{K}_k, \boldsymbol{\delta}_k)} = \begin{cases} \frac{p(r_k+1)}{p(r_k)} \frac{r_k+1}{R_k-r_k} \frac{\mathcal{N}(\delta_{k,r_k+1}^*; 0, \tau_k^2)}{\mathcal{N}(0; 0, \tau_k^2)}, & r_k^* = r_k + 1 \\ \frac{p(r_k-1)}{p(r_k)} \frac{R_k-r_k+1}{r_k} \frac{\mathcal{N}(0; 0, \tau_k^2)}{\mathcal{N}(\delta_{k,J}; 0, \tau_k^2)}, & r_k^* = r_k - 1 \\ \frac{\mathcal{N}(\delta_{k,r_k+1}^*; 0, \tau_k^2)}{\mathcal{N}(\delta_{k,J}; 0, \tau_k^2)}, & r_k^* = r_k, \end{cases}$$

where σ^2 is the proposal variance for the basis coefficients. For the special cases where $r_k = 0$ or $r_k = R_k$, the respective proposal ratios can be shown to be $R_k/(3\mathcal{N}(\delta_{k,r_k+1}^*; 0, \sigma^2))$ and $(R_k\mathcal{N}(\delta_{k,J}; 0, \sigma^2))/3$.

Proof: See Supplement S5.

Algorithm 1 RJMCMC Algorithm

- 1: **for** $i \leftarrow 1$ **to** b **do**
 - 2: Metropolis-Hastings updates for $\boldsymbol{\beta}_k$, ϵ_k , and $\boldsymbol{\gamma}$
 - 3: Gibbs updates for τ_k^2 and ρ^2
 - 4: **for** Partition $k \leftarrow 1$ **to** K **do**
 - 5: Propose to: (1) add; (2) remove; or (3) move a knot with equal probability $1/3$
 - 6: Denote proposed vector of knots and coefficients as \mathcal{K}_k^* and $\boldsymbol{\delta}_k^*$, respectively
 - 7: Generate $U \sim \text{Unif}(0, 1)$
 - 8: Accept \mathcal{K}_k^* and $\boldsymbol{\delta}_k^*$ if $U < \min\{1, \alpha\}$ where α is defined in (6).
 - 9: **end for**
 - 10: **end for**
-

3.4 Prediction

Let n_o denote the number of observations used for model-fitting and let n_p denote the number of observations used for validation. Upon fitting the hierarchical spatial model on the vector of observed locations $\mathcal{S}_o = (\mathbf{s}_1, \dots, \mathbf{s}_{n_o})$, a natural extension is to infer the linear predictor $\eta(\cdot)$ at a vector of prediction locations $\mathcal{S}_p = (\mathbf{s}_1, \dots, \mathbf{s}_{n_p})$. Letting $\mathbf{s}^* \in \mathcal{S}_p$ be an

arbitrary unobserved location residing in partition k , we write:

$$\eta(\mathbf{s}^*) = \mathbf{x}_k(\mathbf{s}^*)^\top \boldsymbol{\beta}_k + \boldsymbol{\Phi}_k(\mathbf{s}^*; \epsilon_k, \mathcal{K}_k)^\top \boldsymbol{\delta}_k + \mathbf{H}_k(\mathbf{s}^*)^\top \boldsymbol{\gamma},$$

where $\mathbf{x}_k(\mathbf{s}^*)$ is the covariate vector evaluated at location \mathbf{s}^* , $\boldsymbol{\Phi}_k(\mathbf{s}^*; \epsilon_k, \mathcal{K}_k)$ is the adaptive basis function vector with corresponding basis coefficients $\boldsymbol{\delta}_k$, and $\mathbf{H}_k(\mathbf{s}^*)$ is the global basis function vector with corresponding global basis coefficients $\boldsymbol{\gamma}$. We approximate the posterior predictive distribution for $\eta(\mathbf{s}^*)$ using posterior samples $\{\boldsymbol{\beta}_k, \epsilon_k, \boldsymbol{\delta}_k, \mathcal{K}_k, \boldsymbol{\gamma}\}$. As with the parameter estimation, we note that the predictions are made within each cluster and hence can be done in parallel to promote computational efficiency. Furthermore, the posterior distribution allows for uncertainty quantification by evaluating the variance of the posterior samples.

3.5 Implementation Details

Our method requires tuning three parameters: (1) the number of partitions K ; (2) the prior rate parameter λ for the number of basis functions to be used within each partition; and (3) the prior distribution for the partition-specific bandwidths $\boldsymbol{\epsilon} = \{\epsilon_k\}_{k=1}^K$. Specifying fewer partitions (small K) may not be adequate for approximating nonstationary spatial processes because there may be several heterogeneous subregions within the spatial domain. Conversely, increasing the number of partitions (large K) may create multiple partitions containing very few observation locations (small n_k), potentially yielding a flat spatial surface. For practitioners, we suggest searching over a range of possible values. Specifically $K \in \{K_{\min}, \dots, K_{\max}\}$, where $K_{\min} = \max\{4, \lceil \log_{10}(n) \rceil\}$, and K_{\max} is the largest value of K such that each partition contains at least 50 observations. We set the minimum

value of K to be at least four because there are four global basis functions with the largest bandwidths. If cross validation is not feasible, one could use Akaike’s information criterion (AIC), the Schwarz-Bayesian criterion (BIC), or adjusted R^2 from a model that includes the covariates, global basis functions, and cluster assignment as predictors. For instance, one can initially cluster observations using $K = \max\{4, \lceil \log_{10}(n) \rceil\}$ clusters and then incrementally increase K either until the decrease in AIC is negligible (using the so-called “elbow” method) or until K_{\max} is reached. An example of this procedure is provided in the supplement. In our simulation study, we compare the performance of our method with various choices of K . In fact, our method is fast enough such that practitioners can explore multiple K settings and ultimately choose the most accurate K based on out-of-sample predictions.³

For the partition-specific bandwidths, we specify a uniform prior $\epsilon_k \sim \text{Unif}(\alpha, \beta)$ to allow for control over the range of possible values ϵ_k can take on. For $\mathcal{D} = [0, 5]^2$, a sensitivity analysis suggests that $\alpha = 0.01$ and $\beta = 3$ provides a suitable range of values for ϵ_k to accommodate both smooth and rough partitions. A truncated Poisson distribution with prior rate parameter λ is used for the number of basis functions for each partition. A sensitivity analysis suggests that results are relatively insensitive to choices of λ in the range 5-20 so we choose $\lambda = 5$ to promote parsimony and computational efficiency. We set the priors for $\boldsymbol{\beta}$ and τ_k^2 following (Hughes and Haran, 2013): $\boldsymbol{\beta} \sim \mathcal{N}(\mathbf{0}, 100\mathbf{I})$ and $\tau_k^2 \sim \text{IG}(0.5, 2000)$. The latter prior is desirable because it corresponds to the prior belief that the fixed effects are sufficient for explaining the data. For the global basis function matrix \mathbf{H} , we use three layers of nested bisquare basis functions (Sengupta et al., 2016).

4 Simulation Study

In this section, we demonstrate the Adapt-BaSeS approach through an extensive simulation study featuring multiple spatial data classes and dependence structures. To benchmark performance, we compare our approach with two competing methods.

4.1 Simulation Study Design

Let $\mathbf{s}_i \in \mathcal{D} = [0, 5]^2 \subset \mathbb{R}^2$ for $i = 1, \dots, n$ denote the spatial locations and let $\mathcal{S} = (\mathbf{s}_1, \dots, \mathbf{s}_n)$. On these locations, let $\mathbf{z} = (z(\mathbf{s}_1), \dots, z(\mathbf{s}_n))^\top$ denote the vector of response variables (i.e., the data). For model fitting, we use $n_o = 5,000$ observations and reserve $n_p = 1,000$ observations for validation. We consider both binary and count data, with the associated spatial random effects generated from both nonstationary and stationary spatial processes. Observations are generated using the SGLMM framework described in (1) with $x_1, x_2 \sim \text{Unif}(-0.5, 0.5)$ and $\boldsymbol{\beta} = (1, 1)$. We study our method for $K = \{9, 16, 25, 36, 49\}$ partitions. All together, we study a total of $5 \times 2 \times 2 = 20$ implementations.

The nonstationary spatial random effects $\mathbf{w} = \{w(\mathbf{s}_i) : \mathbf{s}_i \in \mathcal{D}\}$ are generated by smoothing several locally stationary processes (Fuentes, 2001). Further details are provided in the supplementary material. The stationary spatial random effects are generated using an exponential covariance function with scaling parameter $\phi = 1$ and partial sill parameter $\sigma^2 = 1$. The binary datasets use a Bernoulli data model and a logit link function and the count datasets are generated using a Poisson data model and a log link function. For each data generation mechanism (4 total), we generate 100 replicate data sets.

We fit the model using the hierarchical framework outlined in (5). We generate 100,000 samples from the posterior distribution $\pi(\boldsymbol{\beta}, \epsilon_k, \mathcal{K}_k, \boldsymbol{\delta}_k, \tau_k^2, \rho^2)$ for $k = 1, \dots, K$ using the RJMCMC algorithm described in Algorithm 1. To evaluate predictive performance, we compute the average root cross-validated mean squared prediction error (rCVMSPE), defined as $\text{rCVMSPE} = \left(\frac{1}{n_p} \sum_{i=1}^{n_p} (z_i - \hat{z}_i)^2 \right)^{1/2}$, the area under the receiver operating curve (AUC) for the binary case, and the walltime (computation time) required to run 100,000 iterations of the RJMCMC algorithm.

Fitting a “gold standard” SGLMM (1) is prohibitive due to the overparameterized model and large matrix operations. Hence, we compare our approach with two competing methods: the NNGP approach and a fixed bisquare basis function approach. The computation times are based on a single 2.4 GHz Intel Xeon Gold 6240R processor provided by GMU’s HOPPER high-performance computing infrastructure.

4.2 Simulation Study Results

Table 1 and Table 2, respectively, present the rCVMSPE and AUC for Adapt-BaSeS and the competing approaches. The results indicate that our method yields more accurate predictions than the competing methods across different values of K , data classes, and covariance structures. Paired t -tests were performed to compare the sets of rCVMSPE’s between our approach and the competing methods. The corresponding p -values were found to be statistically significant, with $p < 0.001$ for each pairwise comparison. Predictive performance generally improves as we increase the number of partitions K . However, the predictive standard deviations generally increase with larger K . For one simulated nonstationary

dataset with 50,000 observations, we present the posterior predictive log intensity surface (Figure 2) and the posterior predictive probability surface (Figure 3) obtained from the implementation yielding the lowest rCVMSPE ($K = 49$). Based on a visual inspection, our method successfully captures the nonstationary behavior of the true latent spatial process in both cases. Plots illustrating the prediction standard deviations, posterior differences, and coverage probabilities can be found in the supplementary material. The computation time required to fit the model to this large-scale dataset is 105 minutes on a laptop.

The model-fitting walltimes are reported in the supplementary material. The proposed approach exhibits higher computational costs than the fixed basis function approach. However, our method is more computationally efficient than the NNGP approach. The shorter walltimes for the fixed basis function approach are expected since the spatial basis functions are fixed prior to model-fitting. In contrast, our proposed method modifies the spatial basis functions at each iteration of the RJMCMC algorithm, leading to increased computational costs. Despite the longer walltimes, our approach offers additional flexibility in modeling the latent spatial process and yields more accurate predictions. Importantly, both approaches provide substantial improvements in computational efficiency over the “gold standard” SGLMM (1), which would be computationally infeasible for a dataset with $n_o = 5,000$ observations.

5 Applications

In this section, we apply the Adapt-BaSeS to two real-world spatial datasets: binary incidence of dwarf mistletoe in Minnesota (Hanks, Hooten and Baker, 2011) and counts from

Method	Nonstationary		Stationary	
	Poisson	Binary	Poisson	Binary
Bisquare	1.817 (0.140)	0.478 (0.045)	1.754 (0.143)	0.460 (0.044)
NNGP		0.474 (0.131)		0.458 (0.123)
$K = 9$	1.719 (0.156)	0.470 (0.042)	1.709 (0.128)	0.453 (0.043)
$K = 16$	1.700 (0.174)	0.468 (0.043)	1.650 (0.180)	0.451 (0.042)
$K = 25$	1.688 (0.192)	0.466 (0.045)	1.648 (0.195)	0.450 (0.044)
$K = 36$	1.682 (0.206)	0.465 (0.048)	1.639 (0.213)	0.449 (0.047)
$K = 49$	1.680 (0.224)	0.464 (0.052)	1.633 (0.232)	0.448 (0.051)

Table 1: Average rCVMSPE for the simulation study. Columns correspond to the data class and spatial dependence structure. Results are presented for various choices of K . Top rows correspond to the fixed basis functions approach and NNGP. Average standard deviation of the predictions are provided in parentheses.

Method	Nonstationary	Stationary
Bisquare	0.663	0.711
NNGP	0.679	0.716
$K = 9$	0.693	0.731
$K = 16$	0.700	0.736
$K = 25$	0.706	0.740
$K = 36$	0.709	0.742
$K = 49$	0.711	0.743

Table 2: Out-of-sample area under the receiver operating curve (AUC)

the North American Breeding Bird Survey (BBS) (Ziolkowski et al., 2022).

5.1 Binary Data: Parasitic Infestation of Dwarf Mistletoe

The dwarf mistletoe is a parasitic species that extracts key resources from its host, such as the black spruce species (Geils and Hawksworth, 2002). This infestation poses economic challenges, because black spruce is a valuable resource for producing high-quality paper. Thus, identifying regions with high probability of dwarf mistletoe being present would

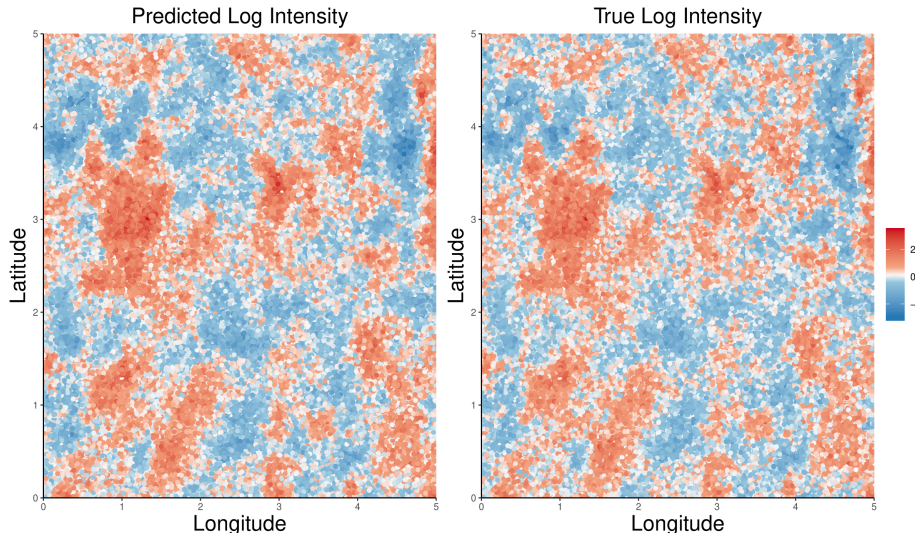


Figure 2: Predicted (left) and true (right) log intensity surface for one nonstationary validation sample for the count data case.

allow for targeted management and control efforts. We apply our method to analyze dwarf mistletoe incidence data in Minnesota, obtained from the Minnesota Department of Natural Resources operational inventory (Hanks, Hooten and Baker, 2011). The dataset contains binary incidence of dwarf mistletoe at $n = 25,431$ locations, with dwarf mistletoe being present at 2,872 of these locations. We fit the model on $n_o = 12,931$ observations and set aside $n_p = 12,500$ observations for validation. We consider several covariates as inputs to our model, including: (1) the average age of trees in years; (2) basal area per acre of trees in the stand; (3) average canopy height; and (4) volume of the stand measured in cords. We study the performance of our method for $K \in \{9, 16, 25, 36, 49\}$.

For each implementation, we compute the rCVMSPE and the AUC for the binary classification (Table 3). We observe that increasing the number of partitions improves the predictive performance of our proposed approach. Specifically, using $K = 49$ partitions yields the highest AUC value and the lowest rCVMSPE. In contrast, the fixed basis function

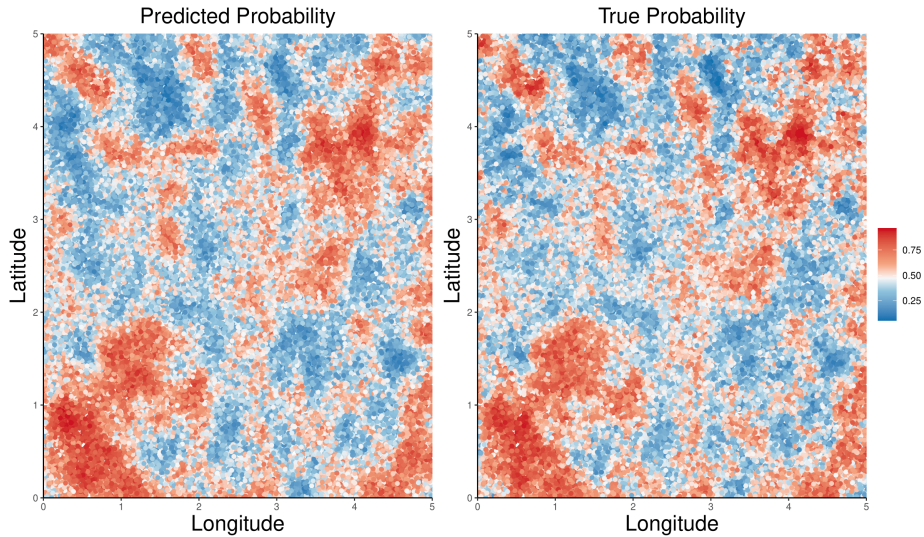


Figure 3: Predicted (left) and true (right) probability surface for one nonstationary validation sample for the binary data case.

approach provides less accurate predictions compared to our proposed method, across all five partition levels. Figure 4 displays the predictive probability surface and the true binary observations for the validation sample, for the case of $K = 49$. The predictive probability map aligns with results from a previous study (Hanks, Hooten and Baker, 2011) where dwarf mistletoe is abundant in the northwestern and middle eastern parts of northern Minnesota. Our results suggest that there are higher probabilities of dwarf mistletoe occurrence in these regions; hence, conservation hubs can be established there.

5.2 Count Data: North American Breeding Bird Survey 2018

The Breeding Bird Survey (BBS) is an annual roadside survey that involves trained observers monitoring the abundance of bird populations in North America (Ziolkowski et al., 2022). The bird surveys are conducted along more than 3,000 routes across the continental US, with 50 stops per route spaced roughly 0.5 miles apart. At each stop, observers

Method	rCVMSPE	AUC
Bisquare	0.308 (0.015)	0.734
$K = 9$	0.300 (0.017)	0.764
$K = 16$	0.296 (0.022)	0.785
$K = 25$	0.295 (0.023)	0.790
$K = 36$	0.294 (0.024)	0.793
$K = 49$	0.293 (0.025)	0.795

Table 3: rCVMSPE and AUC for the dwarf mistletoe dataset. Results are presented for varying number of partitions K . The top row corresponds to the fixed basis function approach. The average standard deviation of the predictions are provided in parentheses.

conduct a three-minute point count where they record the total number of birds heard or seen (Pardieck et al., 2016). We used the sum of counts from the 50 stops in one year’s survey as an index of species abundance along the route for that specific year. Modeling species abundance is essential for informing resource management decisions, such as implementing sustainable harvesting practices or guiding habitat restoration efforts. For example, monitoring bird abundance has been fundamental to many successful programs aimed at studying and conserving bird populations (Brown, Hickey, and Harrington, 2000). The particular BBS dataset includes Blue Jay (*Cyanocitta cristata*) bird counts at a total of $n = 1,593$ locations, covering eastern and central regions of the United States. We use $n_o = 1,000$ observations to fit the model and reserve $n_p = 593$ for validation. The BBS data set does not provide any covariates, but environmental predictors can be obtained from various data sources. While this is a demonstration of our approach on a real-world dataset, future ecological studies can benefit from including covariates from multi-modal sources such as temperature, tree cover, and urban indices. We fit the model with only the spatial random effects (i.e., the conditional mean is modeled as $g(\mathbb{E}[z(\mathbf{s}_i)]) = w(\cdot)$ and

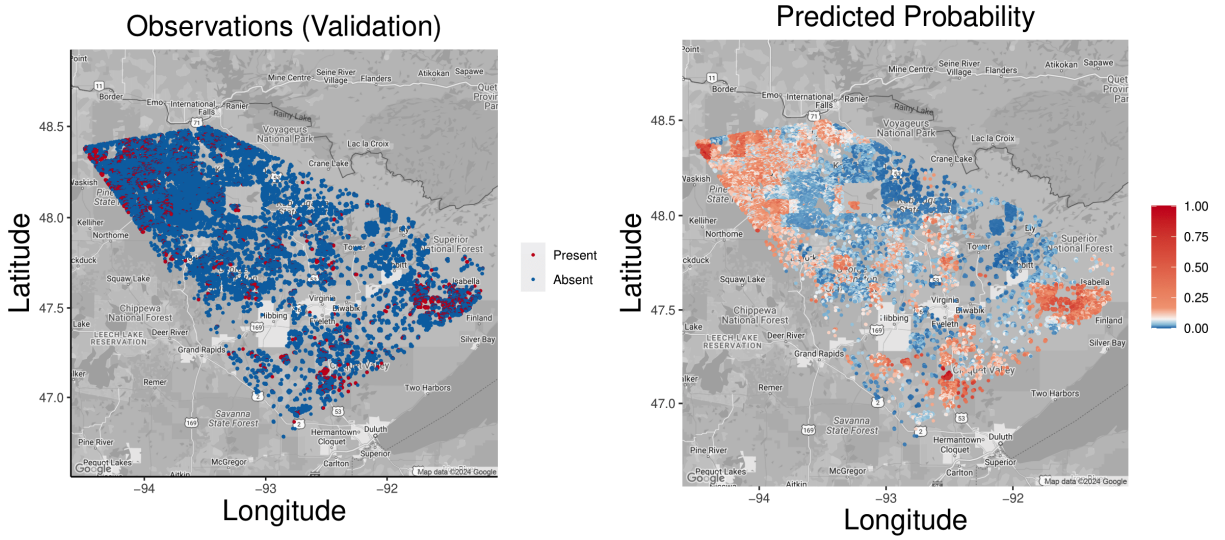


Figure 4: Illustration of the dwarf mistletoe occurrence dataset for $K = 49$. True observations (left) and posterior predictive probability surface (right) for the validation sample. Red points indicate the presence of dwarf mistletoe, while blue points indicate its absence (left plot). Similarly, red points indicate a high predicted probability of dwarf mistletoe, while blue points indicate a low predicted probability (right plot).

does not include spatial covariates).

Table 4 displays the rCVMSPE for each implementation. We find that our method consistently outperforms the fixed basis function approach. For the case of $K = 8$ partitions, Figure 5 displays the true count observations and the predictive intensity surface, obtained from k -fold cross-validation. The predictive intensity map aligns with the observation of large counts in the southwestern and northeastern regions of the eastern United States. This pattern is consistent with the migratory behavior of Blue Jays, which migrate southwestward in the fall and northeastward in the spring in the eastern United States (Gill, 1941). Our results can inform ecological and conservation policies, such as habitat protection and restoration, land-use planning, pesticide regulation, and curtailing the growth of invasive species. The higher intensity values in the northeast and southwestern regions of the eastern United States suggest that more resources should be allocated to the origin and

destination of the migratory paths.

Method	rCVMSPE
Bisquare	8.735 (0.706)
$K = 5$	8.599 (0.735)
$K = 6$	8.583 (0.857)
$K = 7$	8.537 (0.892)
$K = 8$	8.515 (1.013)
$K = 9$	8.572 (0.904)

Table 4: rCVMSPE for the Blue Jay spatial count dataset. Results are presented for varying K . Results from fixed basis functions are in the top row. Average standard deviation of predictions are in parentheses.

6 Discussion

We propose a data-informed, flexible, and computationally efficient method to model high-dimensional non-Gaussian spatial observations with nonstationary spatial dependence structures. Past studies have used spatial radial basis functions; thereby accounting for non-stationarity and reducing computational costs. However, these studies generally fix crucial components of the basis functions, such as the number of basis functions, placement of basis knots, and bandwidth (smoothing) parameters, perhaps arbitrarily, before fitting the model.

Our fast yet flexible method partitions the spatial domain into disjoint subregions using an agglomerative spatial clustering algorithm (Heaton, Christensen and Terres, 2017). We then employ a RJMCMC algorithm to select critical features (knots and bandwidths) of the basis functions within each partition. Results from both our simulation study and real-world applications demonstrate that our approach performs well in both inference and

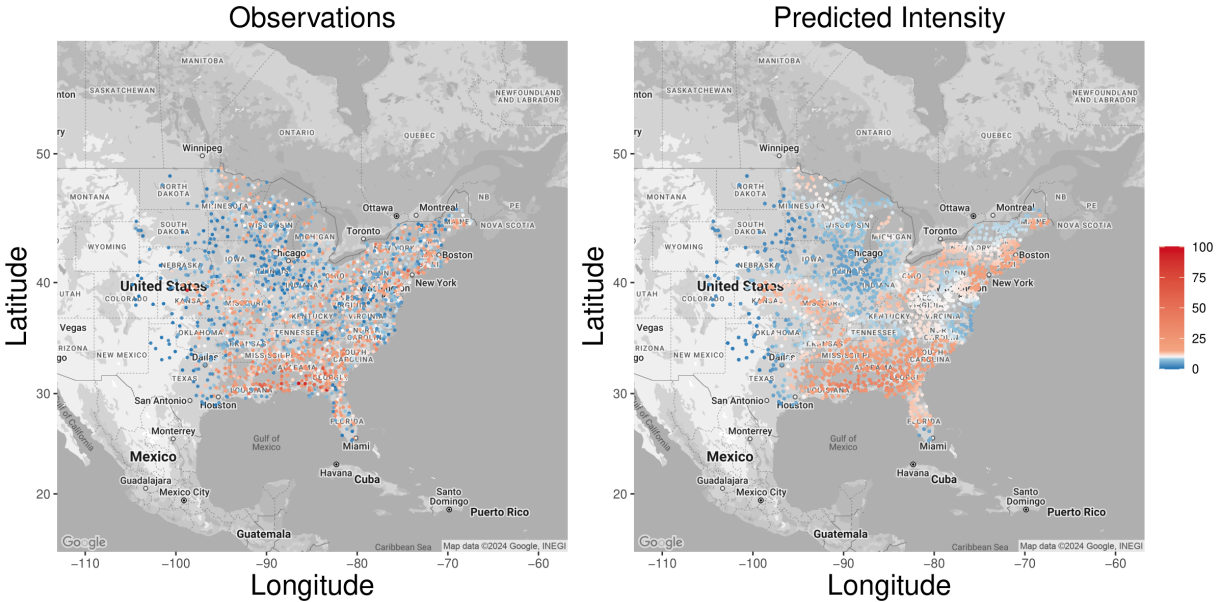


Figure 5: Illustration of the Blue Jay count dataset for $K = 8$. True observations (left) and posterior predictive intensity surface (right). Red points indicate a high abundance of Blue Jays, while blue points indicate a low abundance (left plot). Similarly, red points indicate a high predicted intensity of Blue Jays, while blue points indicate a low predicted intensity (right plot).

predictions over competing methods, while also preserving computational efficiency.

While our proposed adaptive framework primarily focuses on Gaussian radial basis functions, it can be extended to accommodate a wider range of radial basis functions. This includes thin-plate-spline basis functions, multiquadric radial basis functions, and bisquare basis functions, among others. Though our approach offers a significant speedup compared to the “gold standard” SGLMM (1), the computational speedup can be further enhanced by embedding sparse basis functions such as the Wendland basis functions (Nychka et al., 2015) or multi-resolution approximation (M-RA) basis functions (Katzfuss, 2017), which can drastically reduce the number of floating point operations. In a similar strain, the

embarrassingly parallel matrix operations can be distributed across available processors (Guan and Haran, 2018) in high-performance computing systems.

The spatial statistics trinity refers to three key components that are fundamental to spatial analysis: population, sample, and inference (Wang, Gao, and Stein, 2020). This study assumes that the data are collected from an unbiased sample and the population exhibits spatial autocorrelation. A biased sample can introduce biases in the model parameters and predictions (Ravishankar et al., 2023) and lead to less accurate estimates (Johnston et al., 2020). While our approach focuses on estimation, addressing sample conditions (such as biased samples) and population characteristics could be a natural extension for a future study. To address the error caused by a biased sample, existing approaches include creating synthetic data using imputation techniques in undersampled subregions or subsampling from oversampled subregions to make the sample more representative of the population (Li et al., 2017). Alternatively, employing weights can explicitly account for spatially biased presence-only datasets in species distribution modeling (Stolar and Nielsen, 2015; Johnston et al., 2020). Formal model-based approaches (Diggle, Menezes, and Su, 2010; Conn, Thorson, and Johnson, 2017) jointly model the state variable of interest and the sampling site selection processes.

Supplementary Material

The supplementary material includes: (1) details on the construction of the bisquare basis functions as well as a visualization of the multi-resolution “quad-tree” structure; (2) details on the clustering algorithm (Heaton, Christensen and Terres, 2017); (3) model-fitting

walltimes for the simulation study; (4) a proof of the detailed balance proposition; (5) visualizations of the prediction standard deviation surfaces, posterior differences, and coverage probabilities; (6) a recommended procedure and demonstration for choosing the number of partitions K ; (7) standard deviation surfaces for the real-world applications; and (8) inference results for the dwarf mistletoe data example.

Acknowledgements

The authors are grateful to Matthew Heaton, Murali Haran, Jaewoo Park, and Yawen Guan for providing helpful discussions as well as providing sample code. This project was supported by computing resources provided by the Office of Research Computing at George Mason University (<https://orc.gmu.edu>) and funded in part by grants from the National Science Foundation (Awards Number 1625039 and 2018631).

References

- Baker, E., Barbillon, P., Fadikar, A., Gramacy, R. B, Herbei, R., Higdon, D., Huang, J., Johnson, L. R., Ma, P., Mondal, A., and others (2022). Analyzing stochastic computer models: A review with opportunities. *Statistical Science* **37(1)**, 64–89.
- Banerjee, S., Carlin, B. P. and Gelfand, A. E. (2003). *Hierarchical Modeling and Analysis for Spatial Data*. 2nd Edition. Chapman and Hall/CRC, New York.
- Banerjee, S., Gelfand, A. E., Finley, A. O. and Sang, H. (2008). Gaussian predictive process

- models for large spatial data sets. *Journal of the Royal Statistical Society: Series B (Statistical Methodology)* **70(4)**, 825–848.
- Banerjee, S., Gelfand, A. E., and Sirmans, C. F. (2003). Directional rates of change under spatial process models. *Journal of the American Statistical Association* **98(464)**, 946–954.
- Billier, C. (2000). Adaptive Bayesian regression splines in semiparametric generalized linear models. *Journal of Computational and Graphical Statistics* **9(1)**, 122–140.
- Bradley, J. R., Cressie, N. and Shi, T. (2011). Selection of rank and basis functions in the spatial random effects model. In *Proceedings of the 2011 Joint Statistical Meetings*, 3393-3406. Alexandria, VA: American Statistical Association.
- Brockmann, M., Gasser, T., and Herrmann, E. (1993). Locally adaptive bandwidth choice for kernel regression estimators. *Journal of the American Statistical Association* **88(424)**, 1302–1309.
- Brooks, S., Gelman, A., Jones, G., and Meng, X. L. (2011). *Handbook of Markov Chain Monte Carlo*. Chapman and Hall/CRC, Boca Raton.
- Brown, S. C., Hickey, C., and Harrington, B. (2000). *United States shorebird conservation plan*. Manomet Center for Conservation Sciences.
- Chaudhuri, A., Kakde, D., Sadek, C., Gonzalez, L. and Kong, S. (2017). The mean and median criteria for kernel bandwidth selection for support vector data description. In

2017 IEEE International Conference on Data Mining Workshops (ICDMW), 842-849.

New Orleans, LA: Institute of Electrical and Electronics Engineers.

Christensen, O. F., Roberts, G. O., and Sköld, M. (2006). Robust Markov chain Monte Carlo methods for spatial generalized linear mixed models. *Journal of Computational and Graphical Statistics* **15(1)**, 1–17.

Conn, P. B., Thorson, J. T., and Johnson, D. S. (2017). Confronting preferential sampling when analysing population distributions: diagnosis and model-based triage. *Methods in Ecology and Evolution* **8(11)**, 1535–1546.

Cressie, N. (1993). *Statistics for Spatial Data: Wiley Series in Probability and Statistics*. Revised Edition. John Wiley & Sons, New York.

Cressie, N. and Johannesson, G. (2006). Spatial prediction for massive datasets. In *Mastering the Data Explosion in the Earth and Environmental Sciences: Proceedings of the Australian Academy of Science Elizabeth and Frederick White Conference*, 1–11. Canberra, Australia: Australian Academy of Science.

Cressie, N. and Johannesson, G. (2008). Fixed rank kriging for very large spatial data sets. *Journal of the Royal Statistical Society: Series B (Statistical Methodology)* **70(1)**, 209–226.

Cressie, N., Sainsbury-Dale, M. and Zammit-Mangion, A. (2022). Basis-function models in spatial statistics. *Annual Review of Statistics and Its Application* **9**, 373–400.

- Cressie, N. and Wikle, C. K. (2011). *Statistics for Spatio-Temporal Data*. 1st Edition. John Wiley & Sons, Hoboken.
- Cressie, N. and Wikle, C. K. (2015). *Statistics for Spatio-Temporal Data*. John Wiley & Sons.
- Damodaran, B. B. (2018). Fast optimal bandwidth selection for RBF kernel using reproducing kernel Hilbert space operators for kernel based classifiers. *arXiv preprint arXiv:1804.05214*.
- Datta, A., Banerjee, S., Finley, A. O. and Gelfand, A. E. (2016). Hierarchical nearest-neighbor Gaussian process models for large geostatistical datasets. *Journal of the American Statistical Association* **111(514)**, 800–812.
- Denis, M and Molinari, N. (2010). Free knot splines with RJMCMC in survival data analysis. *Communications in Statistics—Theory and Methods* **39(14)**, 2617–2629.
- Diggle, P. J., Menezes, R., and Su, T. L. (2010) Geostatistical inference under preferential sampling. *Journal of the Royal Statistical Society Series C: Applied Statistics* **59(2)**, 191–232.
- Diggle, P. J., Tawn, J. A. and Moyeed, R. A. (1998). Model-based geostatistics. *Journal of the Royal Statistical Society: Series C (Applied Statistics)* **47(3)**, 299–350.
- Dovers, E., Brooks, W., Popovic, G. C. and Warton, D. I. (2023). Fast, approximate maximum likelihood estimation of log-Gaussian Cox processes. *Journal of Computational and Graphical Statistics*, 1–11.

- Ejigu, B. A., Wencheko, E., Moraga, P. and Giorgi, E. (2020). Geostatistical methods for modelling non-stationary patterns in disease risk. *Spatial Statistics* **35**, 100397–100415.
- Ferkingstad, E. and Rue, H. (2015). Improving the INLA approach for approximate Bayesian inference for latent Gaussian models. *Electronic Journal of Statistics* **9(2)**, 2706-2731.
- Finley, A. O., Sang, H., Banerjee, S. and Gelfand, A. E. (2009). Improving the performance of predictive process modeling for large datasets. *Computational Statistics & Data Analysis* **53(8)**, 2873–2884.
- Fuentes, M. (2001). A high frequency kriging approach for non-stationary environmental processes. *Environmetrics* **12(5)**, 469–483.
- Furrer, R., Genton, M. G. and Nychka, D. (2006). Covariance tapering for interpolation of large spatial datasets. *Journal of Computational and Graphical Statistics* **15(3)**, 502–523.
- Gamerman, D. (1997). Sampling from the posterior distribution in generalized linear mixed models. *Statistics and Computing* **7**, 57–68.
- Geils, B. W. and Hawksworth, F. G. (2002). Damage, effects, and importance of dwarf mistletoes. In *US Department of Agriculture, Forest Service, Rocky Mountain Research Station*, Chapter 5, 57-65. Ogden, UT.
- Gill, G. (1941). Notes on the migration of Blue Jays. *Bird-Banding*, 109–112.
- Green, P. J. (1995). Reversible jump Markov chain Monte Carlo computation and Bayesian model determination. *Biometrika* **82(4)**, 711–732.

- Guan, Y. and Haran, M. (2018). A computationally efficient projection-based approach for spatial generalized linear mixed models. *Journal of Computational and Graphical Statistics* **27(4)**, 701–714.
- Hanks, E. M., Hooten, M. B. and Baker, F. A. (2011). Reconciling multiple data sources to improve accuracy of large-scale prediction of forest disease incidence. *Ecological Applications* **21(4)**, 1173–1188.
- Haran, M. (2011). Gaussian random field models for spatial data. In *Handbook of Markov Chain Monte Carlo*, 449–478. Chapman and Hall/CRC, Boca Raton.
- Haran, M., Hodges, J. S. and Carlin, B. P. (2003). Accelerating computation in Markov random field models for spatial data via structured MCMC. *Journal of Computational and Graphical Statistics* **12(2)**, 249–264.
- Heaton, M. J., Christensen, W. F. and Terres, M. A. (2017). Nonstationary Gaussian process models using spatial hierarchical clustering from finite differences. *Technometrics* **59(1)**, 93–101.
- Heaton, M. J., Datta, A., Finley, A. O., Furrer, R., Guinness, J., Guhaniyogi, R., Gerber, F., Gramacy, R. B., Hammerling, D., Katzfuss, M., Lindgren, F., Nychka, D. W., Sun, F. and Zammit-Mangion, A. (2019). A case study competition among methods for analyzing large spatial data. *Journal of Agricultural, Biological and Environmental Statistics* **24**, 398–425.
- Higdon, D. (1998). A process-convolution approach to modelling temperatures in the North Atlantic Ocean. *Environmental and Ecological Statistics* **5(2)**, 173–190.

- Higdon, D., Gattiker, J., Williams, B., and Rightley, M. (2008). Computer model calibration using high-dimensional output. *Journal of the American Statistical Association* **103(482)**, 570–583.
- Holland, D. M., Saltzman, N., Cox, L. H. and Nychka, D. (1999). Spatial prediction of sulfur dioxide in the eastern United States. In *geoENV II-Geostatistics for Environmental Applications: Proceedings of the Second European Conference on Geostatistics for Environmental Applications*, 65–76. Valencia, Spain: Springer Netherlands.
- Hughes, J. and Haran, M. (2013). Dimension reduction and alleviation of confounding for spatial generalized linear mixed models. *Journal of the Royal Statistical Society: Series B (Statistical Methodology)* **75(1)**, 139–159.
- Johnston, A., Moran, N., Musgrove, A., Fink, D., and Baillie, S. R. (2020). Estimating species distributions from spatially biased citizen science data. *Ecological Modelling* **422**, 108927.
- Kato, R. and Shiohama, T. (2009). Model and variable selection procedures for semiparametric time series regression. *Journal of Probability and Statistics* **2009**.
- Katzfuss, M. (2013). Bayesian nonstationary spatial modeling for very large datasets. *Environmetrics* **24(3)**, 189–200.
- Katzfuss, M. (2017). A multi-resolution approximation for massive spatial datasets. *Journal of the American Statistical Association* **112(517)**, 201–214.

- Katzfuss, M. and Cressie, N. (2011). Spatio-temporal smoothing and EM estimation for massive remote-sensing data sets. *Journal of Time Series Analysis* **32(4)**, 430–446.
- Katzfuss, M. and Cressie, N. (2012). Bayesian hierarchical spatio-temporal smoothing for very large datasets. *Environmetrics* **23(1)**, 94–107.
- Kim, H. M., Mallick, B. K., and Holmes, C. C. (2005). Analyzing nonstationary spatial data using piecewise Gaussian processes. *Journal of the American Statistical Association* **100(470)**, 653–668.
- Lee, B. S. and Haran, M. (2022). PICAR: An efficient extendable approach for fitting hierarchical spatial models. *Technometrics* **64(2)**, 187–198.
- Lee, B. S. and Park, J. (2023). A scalable partitioned approach to model massive nonstationary non-Gaussian spatial datasets. *Technometrics* **65(1)**, 105–116.
- Li, D. C., Hu, S. C., Lin, L. S., and Yeh, C. W. (2017). Detecting representative data and generating synthetic samples to improve learning accuracy with imbalanced data sets. *PloS one* **12(8)**.
- Lindgren, F. and Rue, H. (2015). Bayesian spatial modelling with R-INLA. *Journal of Statistical Software* **63(19)**, 1–25.
- Lindgren, F., Rue, H. and Lindström, J. (2011). An explicit link between Gaussian fields and Gaussian Markov random fields: the stochastic partial differential equation approach. *Journal of the Royal Statistical Society: Series B (Statistical Methodology)* **73(4)**, 423–498.

- Mak, S., Sung, C. L., Wang, X., Yeh, S. T., Chang, Y. H., Joseph, V. R., Yang, V., and Wu, C. J. (2018). An efficient surrogate model for emulation and physics extraction of large eddy simulations. *Journal of the American Statistical Association* **113(524)**, 1443–1456.
- Nychka, D., Bandyopadhyay, S., Hammerling, D., Lindgren, F. and Sain, S. (2015). A multiresolution Gaussian process model for the analysis of large spatial datasets. *Journal of Computational and Graphical Statistics* **24(2)**, 579–599.
- Pardieck, K. L., Ziolkowski, D. J., Hudson, M. A. R., and Campbell, K. (2016). North American breeding bird survey dataset 1966-2015, version 2015.0. *U.S. Geological Survey, Patuxent Wildlife Research Center*.
- Politis, D. N. (2003). Adaptive bandwidth choice. *Journal of Nonparametric Statistics* **15(5)**, 517–533.
- Ravishankar, P. and Mo, Q., McFowland III, E., and Neill, D. B. (2023). Provable detection of propagating sampling bias in prediction models. *Proceedings of the AAAI Conference on Artificial Intelligence* **37(8)**, 9562–9569.
- Risser, M. D. (2016). Nonstationary spatial modeling, with emphasis on process convolution and covariate-driven approaches. *arXiv preprint arXiv:1610.02447*.
- Risser, M. D. and Calder, C. A. (2015). Bayesian nonstationary spatial modeling for very large datasets. *arXiv preprint arXiv:1507.08613*.
- Royle, J. A. and Wikle, C. K. (2005). Efficient statistical mapping of avian count data. *Environmental and Ecological Statistics* **12(2)**, 225–243.

- Schabenberger, O. and Gotway, C. A. (2005). *Statistical Methods for Spatial Data Analysis*. 1st Edition. Chapman and Hall/CRC, Boca Raton.
- Sengupta, A. and Cressie, N. (2013). Hierarchical statistical modeling of big spatial datasets using the exponential family of distributions. *Spatial Statistics* **4**, 14–44.
- Sengupta, A., Cressie, N., Kahn, B. H. and Frey, R. (2016). Predictive inference for big, spatial, non-Gaussian data: MODIS cloud data and its change-of-support. *Australian & New Zealand Journal of Statistics* **58(1)**, 15–45.
- Sheather, S. J. and Jones, M. C. (1991). A reliable data-based bandwidth selection method for kernel density estimation. *Journal of the Royal Statistical Society: Series B (Methodological)* **53(3)**, 683–690.
- Stolar, J. and Nielsen, S. E. (2015). Accounting for spatially biased sampling effort in presence-only species distribution modelling. *Diversity and Distributions* **21(5)**, 595–608.
- Vecchia, A. V. (1988). Estimation and model identification for continuous spatial processes. *Journal of the Royal Statistical Society: Series B (Methodological)* **50(2)**, 297–312.
- Wang, J., Gao, B., and Stein, A. (2020). The spatial statistic trinity: A generic framework for spatial sampling and inference. *Environmental Modelling & Software* **134**, 104835.
- Wikle, C. K., Berliner, L. M., and Cressie, N. (1998). Hierarchical Bayesian space-time models. *Environmental and ecological statistics* **5**, 117–154.

- Williams, C. K. and Rasmussen, C. E. (2006). *Gaussian Processes for Machine Learning*. Volume 2. MIT Press, Cambridge.
- Xu, K., Wikle, C. K. and Fox, N. I. (2005). A kernel-based spatio-temporal dynamical model for nowcasting weather radar reflectivities. *Journal of the American Statistical Association* **100(472)**, 1133–1144.
- Zammit-Mangion, A. and Cressie, N. (2018). FRK: An R package for spatial and spatio-temporal prediction with large datasets. *arXiv preprint arXiv:1705.08105*.
- Zhang, H. (2002). On estimation and prediction for spatial generalized linear mixed models. *Biometrics* **58(1)**, 129–136.
- Zilber, D. and Katzfuss, M. (2021). Vecchia–Laplace approximations of generalized Gaussian processes for big non-Gaussian spatial data. *Computational Statistics & Data Analysis* **153**, 107081.
- Ziolkowski Jr., D., Lutmerding, M., Aponte, V. I. and Hudson, M.-A. (2022). *North American Breeding Bird survey dataset 1966-2021: U.S. Geological Survey data release*.

Supplementary Material for Flexible Basis Representations for Modeling Large Non-Gaussian Spatial Data

Remy MacDonald and Ben Seiyon Lee

Department of Statistics, George Mason University

1 Reversible Jump MCMC

Given the challenge of visually determining the appropriate number and placement of knots in spatial data, it is crucial to employ adaptive methods for knot selection. One such method is the reversible jump Markov chain Monte Carlo (RJMCMC) sampler (Green, 1995), which provides a flexible framework for Markov chain Monte Carlo simulation by allowing the dimension of the parameter space to vary at each iteration.

The RJMCMC sampler is particularly useful for model selection tasks, as it enables the Markov chain to explore parameter subspaces of different dimensions. This capability has led to successful application in various domains, including change-point analysis (Fan and Brooks, 2000), finite mixture models (Richardson and Green, 1997), time series models with an unknown number of components (Brooks, Giudici and Roberts, 2003), variable selection in regression models (Nott and Leonte, 2004), and knot selection in curve fitting (Denison, Mallick and Smith, 1998).

Let y be a vector of observations, and let $\mathcal{M} = \{\mathcal{M}_1, \mathcal{M}_2, \dots\}$ denote a countable collection of candidate models, indexed by a model indicator $k \in \mathcal{K}$, for some countable set

\mathcal{K} . Each model \mathcal{M}_k has an n_k -dimensional vector of unknown parameters, $\theta_k \in \Theta_k \subset \mathbb{R}^{n_k}$, where n_k can vary with k . The joint distribution of (k, θ_k, y) is modeled as,

$$p(k, \theta_k, y) = p(k)p(\theta_k | k)p(y | k, \theta_k),$$

where $p(k)$ is the model probability, $p(\theta_k | k)$ is the parameter prior given the model, and $p(y | k, \theta_k)$ is the likelihood. Inference about k and θ_k is based on the joint posterior $p(k, \theta_k | y) \propto p(k, \theta_k, y)$, which is known as the target distribution. For convenience, we abbreviate (k, θ_k) as x , and $p(k, \theta_k | y) = p(x | y)$ as $\pi(x)$. Given k , x lies in $\mathcal{C}_k = \{k\} \times \Theta_k$, while generally, $x \in \mathcal{C} = \bigcup_{k \in \mathcal{K}} \mathcal{C}_k$.

In order to traverse freely across the combined parameter space \mathcal{C} , we need a method that moves between parameter subspaces $\mathcal{A}, \mathcal{B} \subset \mathcal{C}$ of possibly different dimension. To that end, we consider different move types m , and for each of these move types we construct a transition kernel P_m , which satisfies the detailed balance condition,

$$\int_{\mathcal{A}} \int_{\mathcal{B}} \pi(dx) P_m(x, dx') = \int_{\mathcal{B}} \int_{\mathcal{A}} \pi(dx') P_m(x', dx) \quad (1)$$

for all $\mathcal{A}, \mathcal{B} \subset \mathcal{C}$. This means that the equilibrium probability that the state of the chain is in a general set \mathcal{A} and moves to a general set \mathcal{B} is the same as with \mathcal{A} and \mathcal{B} reversed. To construct the MCMC sampler, consider $x = (k, \theta_k)$ to be the current state of the Markov chain. Following the Metropolis-Hastings algorithm, a move of type m is proposed to a new state $x' = (k', \theta_{k'})$ according to the proposal density $q_m(x, dx')$. As usual with the Metropolis-Hastings algorithm, the detailed balance condition (1) is enforced through the acceptance probability, where the move to the candidate state x' is accepted with probability

$$\alpha_m(x, x') = \min \left\{ 1, \frac{\pi(dx') q_m(x', dx)}{\pi(dx) q_m(x, dx')} \right\},$$

otherwise, remain at the current state x . At each step of the RJMCMC algorithm, Brooks et al. (2011) divide the types of moves m into two major categories:

- *Within-model moves*: fix the model index k and update the parameters θ_k following standard Gibbs or Metropolis-Hastings algorithms.
- *Between-model moves*: jointly update the state $x = (k, \theta_k)$ by proposing a new state $x' = (k', \theta'_{k'}) \sim q_m(x, dx')$ and “matching dimensions” before accepting with probability $\alpha_m(x, x')$.

While the within-model moves are straightforward, the between-moves are more complicated as they involve a “dimension matching” component (Green, 1995). Suppose that the current state $x = (k, \theta_k)$ has dimension n_k under the current model \mathcal{M}_k , and the proposed state $x' = (k', \theta'_{k'})$ under model $\mathcal{M}_{k'}$ has dimension $n_{k'}$, where $n_k \neq n_{k'}$. In order to “match dimensions” between the two model states, introduce an auxiliary variable for the transition m from model \mathcal{M}_k to model $\mathcal{M}_{k'}$ denoted $u \sim g_m$ and of dimension r_m where the density g_m is known. The new state $\theta'_{k'}$ is constructed as $(\theta'_{k'}, u') = h_m(\theta_k, u)$ for some suitable deterministic function h_m . The reverse move from x' to x needs to be defined symmetrically by generating random numbers u' of dimension r'_m from the joint distribution g'_m needed for the reverse move, to move from $\theta'_{k'}$ to θ_k , using the inverse function h'_m of h_m . In order for the transformation from (θ_k, u) to $(\theta'_{k'}, u')$ to be a diffeomorphism, meaning the transformation and its inverse are differentiable, it must be the case that $n_k + r_m = n_{k'} + r'_m$.

When there are multiple possible moves m , we must generally also include the probability j_m of choosing a specific move. The detailed balance requirement (1) can then be rewritten as

$$\int_{\mathcal{A}} \int_{\mathcal{B}} \pi(x) j_m(x) g_m(u) \alpha_m(x, x') dx du = \int_{\mathcal{B}} \int_{\mathcal{A}} \pi(x') j_m(x') g'_m(u') \alpha_m(x', x) dx' du'$$

for all $\mathcal{A}, \mathcal{B} \subset \mathcal{C}$. Thus, a sufficient choice for the acceptance probability α_m corresponding to move type m is given by

$$\alpha_m(x, x') = \min \left\{ 1, \frac{\pi(x') j_m(x') g'_m(u')}{\pi(x) j_m(x) g_m(u)} \left| \frac{\partial(\theta'_{k'}, u')}{\partial(\theta_k, u)} \right| \right\},$$

where the last factor corresponds to the Jacobian for the change of variable between (θ_k, u) and (θ'_k, u') .

2 Bisquare Basis Functions

We employ the bisquare basis functions from (Sengupta and Cressie, 2013; Cressie and Johannesson, 2008) which take the form:

$$\Phi_m(\mathbf{s}) = \left\{ 1 - \left(\frac{\|\mathbf{s} - \mathbf{u}_m\|}{\gamma} \right)^2 \right\}^2 \mathbf{1}(\|\mathbf{s} - \mathbf{u}_m\| < \gamma),$$

where \mathbf{u}_m is the center of basis function m and $\mathbf{1}(\cdot)$ is an indicator function. The knots associated with each basis function are constructed according to a multi-resolution “quad-tree” structure such that the knots associated with different resolutions do not overlap. In particular, we use three resolutions, where there are four knot locations $\mathbf{u}_1, \dots, \mathbf{u}_4$ for the first resolution, 16 knots $\mathbf{u}_5, \dots, \mathbf{u}_{20}$ for the second resolution, and 64 knots $\mathbf{u}_{21}, \dots, \mathbf{u}_{84}$ for the third resolution. An illustration of the three resolutions of knot locations is provided in Figure 1. The bandwidth γ for a specific resolution from Cressie and Johannesson (2008) is given by $\gamma = 1.5 \times$ minimum distance between knot locations. We employ the multi-resolution bisquare basis functions into the Bayesian hierarchical framework for spatial generalized linear mixed models (SLGMMs) as follows:

$$\text{Data Model:} \quad z(\mathbf{s}_i) \mid \eta(\mathbf{s}_i) \sim F(\eta(\mathbf{s}_i))$$

$$g(\mathbb{E}[z \mid \boldsymbol{\beta}, \boldsymbol{\delta}]) := \boldsymbol{\eta} = \mathbf{X}\boldsymbol{\beta} + \boldsymbol{\Phi}\boldsymbol{\delta}$$

$$\text{Process Model:} \quad \boldsymbol{\delta} \mid \tau^2 \sim \mathcal{N}(\mathbf{0}, \tau^2 \mathcal{I})$$

$$\text{Parameter Model:} \quad \boldsymbol{\beta} \sim p(\boldsymbol{\beta}), \tau^2 \sim p(\tau^2),$$

where \mathcal{I} denotes the identity matrix and $\boldsymbol{\Phi}$ denotes the matrix of the multi-resolution bisquare basis functions. The hierarchical model is completed by assigning prior distributions for the model parameters $\boldsymbol{\beta}$ and τ^2 . In the simulation study, we use the following

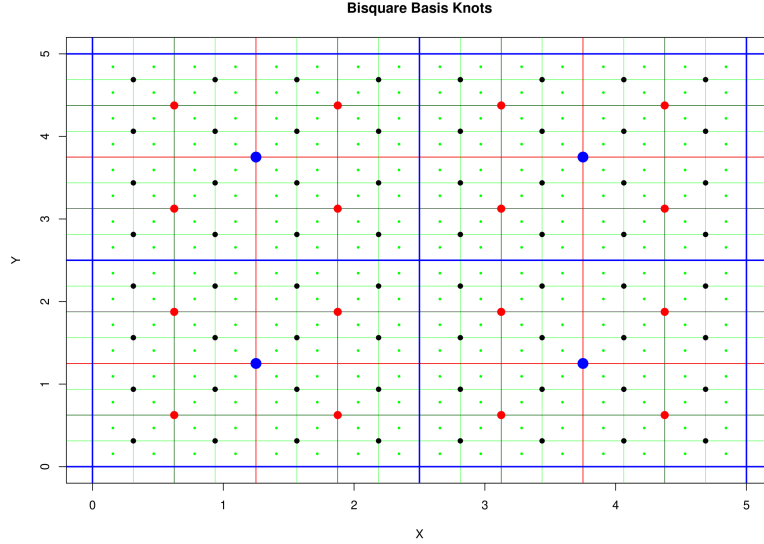


Figure 1: Illustration of multi-resolution quad-tree structure

prior distributions for the model parameters: $\beta \sim \mathcal{N}(\mathbf{0}, 100\mathbf{I})$ and $\tau^2 \sim \text{IG}(0.5, 2000)$.

3 Spatial Clustering Algorithm

Here, we provide details on the clustering algorithm (Heaton, Christensen and Terres, 2017). We obtain residuals ϵ from a nonspatial generalized linear model (GLM) fit with a response vector $\mathbf{z} \in \mathbb{R}^n$ and a covariate matrix $\mathbf{X} \in \mathbb{R}^{n \times m}$. Let $\epsilon_k \in \mathbb{R}^{n_k}$ denote the residuals belonging to the cluster (partition) \mathcal{S}_k . We can then define the dissimilarity between two clusters as

$$d(\mathcal{S}_{k_1}, \mathcal{S}_{k_2}) = \left[\frac{N_{k_1} N_{k_2}}{N_{k_1} + N_{k_2}} (\bar{\epsilon}_{k_1} - \bar{\epsilon}_{k_2})^2 \right] \frac{1}{\bar{E}},$$

where $\bar{\epsilon}_k$ is the average of the residuals in cluster k and \bar{E} is the average Euclidean distance between points in \mathcal{S}_{k_1} and \mathcal{S}_{k_2} amongst Voronoi neighbors. Heaton, Christensen and Terres (2017) define \mathbf{s}_i and \mathbf{s}_j to be Voronoi neighbors if they share a border in a Voronoi tessellation of the observation locations $\mathbf{s}_1, \dots, \mathbf{s}_n$. The spatial clustering algorithm is summarized in Algorithm 1.

Algorithm 1: Spatial clustering algorithm (Heaton, Christensen and Terres, 2017)

- Initialize $\mathcal{S}_k = \mathbf{s}_k$ for $k = 1, \dots, n$ such that each observation is its own cluster.
1. Find clusters $\mathcal{S}_{k_1}, \mathcal{S}_{k_2}$ having the minimum $d(\mathcal{S}_{k_1}, \mathcal{S}_{k_2})$ where $\mathbf{s}_i \sim \mathbf{s}_j$ (Voronoi neighbors) for $\mathbf{s}_i \in \mathcal{S}_{k_1}$ and $\mathbf{s}_j \in \mathcal{S}_{k_2}$
 2. Combine two clusters

$$\mathcal{S}_{\min\{k_1, k_2\}} = \mathcal{S}_{k_1} \cup \mathcal{S}_{k_2}$$

and set

$$\mathcal{S}_{\max\{k_1, k_2\}} = \emptyset$$

Repeat 1-2 until we have K clusters where $K < n$.

We note that Algorithm 1 becomes computationally expensive when the number of observations is large. Following suggestions in Heaton, Christensen and Terres (2017), we perform clustering after aggregating observations to a lattice $\{\mathbf{s}_l^*\}_{l=1}^L$ ($L \ll n$). Here, $\mathcal{N}_l = \{\mathbf{s}_i : \|\mathbf{s}_i - \mathbf{s}_l^*\| < \|\mathbf{s}_i - \mathbf{s}_m^*\| \text{ for all } l \neq m\}$ is the subset of observations whose closest lattice point is \mathbf{s}_l^* , and $\bar{\epsilon}(\mathbf{s}_l^*) = |\mathcal{N}_l|^{-1} \sum_{\mathbf{s}_i \in \mathcal{N}_l} \epsilon(\mathbf{s}_i)$ is the average of the observed residuals in \mathcal{N}_l . We then apply Algorithm 1 to $\{\bar{\epsilon}(\mathbf{s}_l^*)\}_{l=1}^L$ rather than to $\{\epsilon(\mathbf{s}_i)\}_{i=1}^n$. By specifying the number of lattice points L to be much smaller than the number of observations n , the spatial clustering algorithm becomes computationally feasible. For example, in our simulation studies, we specify $L = 400$ for $n = 5,000$.

4 Computation: Model-Fitting Walltimes

In Table 1, we report the model-fitting walltimes (computation times). These include the time required for model initialization and running 100,000 iterations of the RJMCMC algorithm. The proposed approach exhibits higher computational costs compared to the fixed bisquare basis function approach. However, our method is more computationally efficient than the NNGP approach.

Method	Nonstationary		Rough Stationary	
	Poisson	Binary	Poisson	Binary
Fixed (Bisquare)	192	165	184	166
NNGP		2336		2291
$K = 9$	754	581	726	602
$K = 16$	739	633	748	643
$K = 25$	775	715	791	770
$K = 36$	833	830	860	842
$K = 49$	931	926	958	932

Table 1: Average walltime (seconds) for 100,000 iterations

5 Proof of Proposition

In this section, we provide a proof establishing that the acceptance probability satisfies the detailed balance condition for the birth step. Given the r_k knots $\mathcal{K}_k = (\mathbf{u}_{k,1}, \dots, \mathbf{u}_{k,r_k})$, in the birth move we draw a new knot \mathbf{u}^* uniformly with probability $1/(R_k - r_k)$ from the set of the $R_k - r_k$ vacant knot locations. Let $\mathcal{K}_k^* = \mathcal{K}_k \cup \{\mathbf{u}^*\}$ be the proposed set of knots, which now has size $r_k^* = r_k + 1$. The resulting model is now defined by the new model indicator $r_k + 1$, the new knots $\mathcal{K}_k^* = (\mathbf{u}_{k,1}^*, \dots, \mathbf{u}_{k,r_k+1}^*)$ (with $\mathbf{u}_{k,i}^* = \mathbf{u}_{k,i}$ for $i \leq r_k$ and $\mathbf{u}_{k,r_k+1}^* = \mathbf{u}^*$), and the new basis coefficients $\boldsymbol{\delta}_k^* = (\delta_{k,1}^*, \dots, \delta_{k,r_k+1}^*)$, which must be adjusted appropriately. Formally, the birth move can be defined as a transition from state $\theta = (r_k, \theta_{r_k})$ to state $\theta^* = (r_k + 1, \theta_{r_k+1}^*)$. With

$$\theta_{r_k} = (\mathcal{K}_k, \boldsymbol{\delta}_k, \beta_k, \gamma, \tau_k^2, \rho^2, \epsilon_k)$$

and

$$\theta_{r_k+1}^* = (\mathcal{K}_k^*, \boldsymbol{\delta}_k^*, \beta_k, \gamma, \tau_k^2, \rho^2, \epsilon_k),$$

there is a change in dimension from $\dim(\theta_{r_k}) = 2r_k + P + G + 3$ to $\dim(\theta_{r_k+1}^*) = 2r_k + P + G + 5$. For the birth move, we have to compute $\theta_{r_k+1}^*$ as a function of θ_{r_k} and two random

numbers \mathbf{u}^* and u , with $u_B = (\mathbf{u}^*, u)$. The proposed knot \mathbf{u}^* is drawn uniformly with probability $p(\mathbf{u}^*) = 1/(R_k - r_k)$ from the set of the $R_k - r_k$ vacant candidate knots. The new coefficient $\delta_{k,r_{k+1}}^*$ corresponding to the new knot $\mathbf{u}_{k,r_{k+1}}^* = \mathbf{u}^*$ is set equal to u where $u \sim g(u)$, i.e., we simulate a value of u from some proposal distribution g . We specify $u \sim \mathcal{N}(0, \sigma^2)$ where σ^2 can be tuned by the user to achieve a reasonable acceptance rate. Hence, we set

$$\begin{aligned}\delta_{k,r_{k+1}}^* &= u \\ \delta_{k,r_k}^* &= \delta_{k,r_k} \\ &\vdots \\ \delta_{k,1}^* &= \delta_{k,1}\end{aligned}$$

This ensures that in the reverse death move, given the knot $\mathbf{u}_{k,r_{k+1}}^*$ to be deleted, the computation of δ_k from δ_k^* is deterministic and the required dimension matching holds:

$$\begin{aligned}u &= \delta_{k,r_{k+1}}^* \\ \delta_{k,r_k} &= \delta_{k,r_k}^* \\ &\vdots \\ \delta_{k,1} &= \delta_{k,1}^*\end{aligned}$$

The acceptance probability for the birth move can be expressed as

$$\alpha(\theta_{r_k}, \theta_{r_{k+1}}^*) = \min\{1, \mathcal{L} \cdot \mathcal{A} \cdot \mathcal{P} \cdot \mathcal{J}\},$$

where \mathcal{L} is the likelihood ratio, \mathcal{A} is the prior ratio, \mathcal{P} is the proposal ratio, and \mathcal{J} is the Jacobian. The ratio of priors results in

$$\begin{aligned}\mathcal{A} &= \frac{\text{prior for } r_k + 1 \text{ knots}}{\text{prior for } r_k \text{ knots}} \times \frac{\text{prior for location of } r_k + 1 \text{ knots}}{\text{prior for location of } r_k \text{ knots}} \\ &\times \frac{\text{prior for proposed basis coefficient}}{\text{prior for current basis coefficient}} \\ &= \frac{p(r_k + 1)}{p(r_k)} \frac{r_k + 1}{R_k - r_k} \times \frac{\mathcal{N}(\delta_{k,r_k+1}^*; 0, \tau_k^2)}{\mathcal{N}(0; 0, \tau_k^2)},\end{aligned}$$

where the factor $p(r_k+1)/p(r_k)$ depends on the alternative priors of r_k : $p(r_k) \propto \frac{\lambda^{r_k} \exp(-\lambda)}{r_k!} \mathbb{1}_{\{0, \dots, R_k\}}(r_k)$ with prior rate parameter λ . The corresponding proposal ratio \mathcal{P} is given by

$$\begin{aligned}\mathcal{P} &= \frac{d_{r_k+1}(1/(r_k + 1))}{b_{r_k}(1/(R_k - r_k))} \times \frac{1}{\mathcal{N}(\delta_{k,r_k+1}^*; 0, \sigma^2)} \\ &= \frac{d_{r_k+1}(R_k - r_k)}{b_{r_k}(r_k + 1)} \times \frac{1}{\mathcal{N}(\delta_{k,r_k+1}^*; 0, \sigma^2)}.\end{aligned}$$

Considering $\theta_{r_k+1}^*$ as a function of θ_{r_k} and u_B , the Jacobian is

$$\begin{aligned}
\mathcal{J} &= \left| \frac{\partial \theta_{r_k+1}^*}{\partial(\theta_{r_k}, u_B)} \right| \\
&= \begin{vmatrix} \frac{\partial \delta_{k,1}^*}{\partial \delta_{k,1}} & \frac{\partial \delta_{k,2}^*}{\partial \delta_{k,1}} & \frac{\partial \delta_{k,3}^*}{\partial \delta_{k,1}} & \cdots & \frac{\partial \delta_{k,r_k+1}^*}{\partial \delta_{k,1}} \\ \frac{\partial \delta_{k,1}^*}{\partial \delta_{k,2}} & \frac{\partial \delta_{k,2}^*}{\partial \delta_{k,2}} & \frac{\partial \delta_{k,3}^*}{\partial \delta_{k,2}} & \cdots & \frac{\partial \delta_{k,r_k+1}^*}{\partial \delta_{k,2}} \\ \frac{\partial \delta_{k,1}^*}{\partial \delta_{k,3}} & \frac{\partial \delta_{k,2}^*}{\partial \delta_{k,3}} & \frac{\partial \delta_{k,3}^*}{\partial \delta_{k,3}} & \cdots & \frac{\partial \delta_{k,r_k+1}^*}{\partial \delta_{k,3}} \\ \vdots & \vdots & \vdots & \ddots & \vdots \\ \frac{\partial \delta_{k,1}^*}{\partial u} & \frac{\partial \delta_{k,2}^*}{\partial u} & \frac{\partial \delta_{k,3}^*}{\partial u} & \cdots & \frac{\partial \delta_{k,r_k+1}^*}{\partial u} \end{vmatrix} \\
&= \begin{vmatrix} 1 & 0 & 0 & \cdots & 0 \\ 0 & 1 & 0 & \cdots & 0 \\ \vdots & \vdots & \vdots & \ddots & \vdots \\ 0 & 0 & 0 & \cdots & 1 \end{vmatrix} \\
&= 1.
\end{aligned}$$

The proof for both the move and death steps follows similarly.

6 Standard Deviation Surfaces

Figure 2 and Figure 3 illustrate example prediction standard deviation surfaces for the binary and count examples, respectively. It can be noted that regions with high predicted intensity exhibit correspondingly high standard deviations. Conversely, regions with both high and low predicted probabilities demonstrate lower standard deviations.

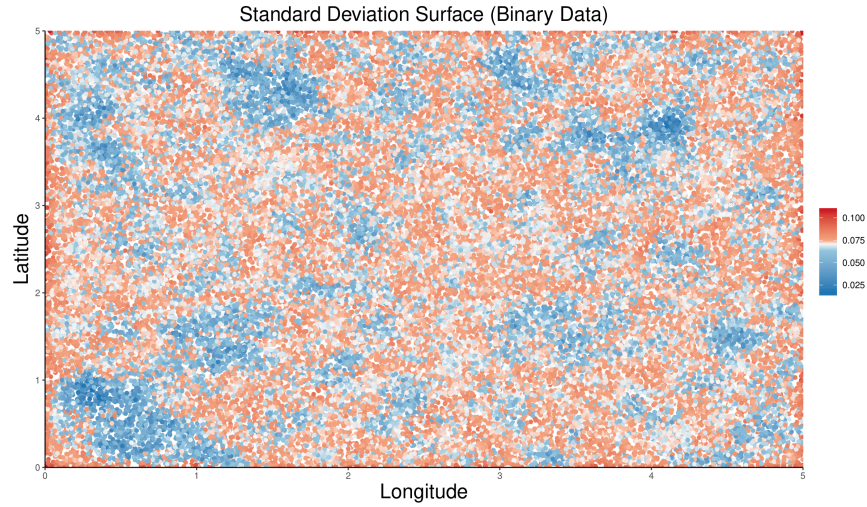


Figure 2: Prediction standard deviation surface for the binary example.

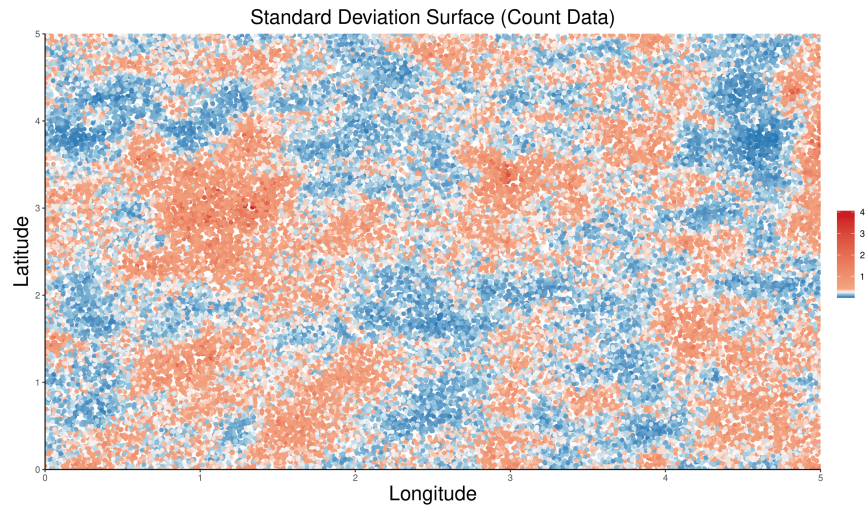


Figure 3: Prediction standard deviation surface for the count example.

7 Generation of Nonstationary Spatial Random Effects

The nonstationary spatial random effects $\mathbf{w} = \{w(\mathbf{s}_i) : \mathbf{s}_i \in \mathcal{D}\}$ are generated by smoothing several locally stationary processes contained in disjoint subregions (Fuentes, 2001). To do this, we partition the spatial domain \mathcal{D} into four disjoint subregions \mathcal{D}_1 , \mathcal{D}_2 , \mathcal{D}_3 , and

\mathcal{D}_4 , where $\mathcal{D}_1 = [0, 2.5]^2$, $\mathcal{D}_2 = [2.5, 5]^2$, $\mathcal{D}_3 = [0, 2.5] \times [2.5, 5]$, and $\mathcal{D}_4 = [2.5, 5] \times [0, 2.5]$. We then specify $C_1(\cdot)$, $C_2(\cdot)$, $C_3(\cdot)$, and $C_4(\cdot)$ to be stationary covariance functions associated with each of the four subregions. Each stationary covariance function comes from the Matérn class with smoothness $\nu = 0.5$, partial sill parameter $\sigma^2 = 1$, and respective range parameters $\phi_1 = 0.5$, $\phi_2 = 0.4$, $\phi_3 = 0.3$, and $\phi_4 = 0.2$. The nonstationary global covariance function is then constructed using the modeling framework of Nott and Dunsmuir (2002), where

$$C(\mathbf{s}, \mathbf{t}) = \sum_{i=1}^4 \lambda_i(\mathbf{s}) \lambda_i(\mathbf{t}) C_i(\mathbf{s}, \mathbf{t}).$$

Here $\lambda_i(\mathbf{s})$ is a weight function based on the distance between location \mathbf{s} and the center of subregion \mathcal{D}_i which we denote as $\boldsymbol{\mu}_i$. The weight function is chosen such that $\lambda_i(\mathbf{s}) \geq 0$, $\sum_{i=1}^4 \lambda_i(\mathbf{s}) = 1$, $\lambda_i(\mathbf{s})$ attains its maximum at $\boldsymbol{\mu}_i$, and decays smoothly to zero as $\|\mathbf{s} - \boldsymbol{\mu}_i\| \rightarrow \infty$. To ensure that $\lambda_i(\mathbf{s}) \geq 0$, Nott and Dunsmuir (2002) employ the kernel function

$$\kappa_\eta(\mathbf{t}) = \exp\left(-\frac{\|\mathbf{t}\|^2}{\eta}\right),$$

where η is a smoothing parameter (we specify $\eta = 6$), and then

$$\lambda_i(\mathbf{s}) = \frac{\kappa_\eta(\mathbf{s} - \boldsymbol{\mu}_i)}{\sum_{j=1}^4 \kappa_\eta(\mathbf{s} - \boldsymbol{\mu}_j)}.$$

8 Posterior Difference Surfaces

For one simulated nonstationary dataset, Figure 4 and Figure 5 below display the posterior difference in the log intensities for the count data case, as well as the posterior difference in probabilities for the binary data case. There does not appear to be any discernible spatial pattern in the difference surfaces in either case. These are due to properties of the binomial and Poisson distribution.

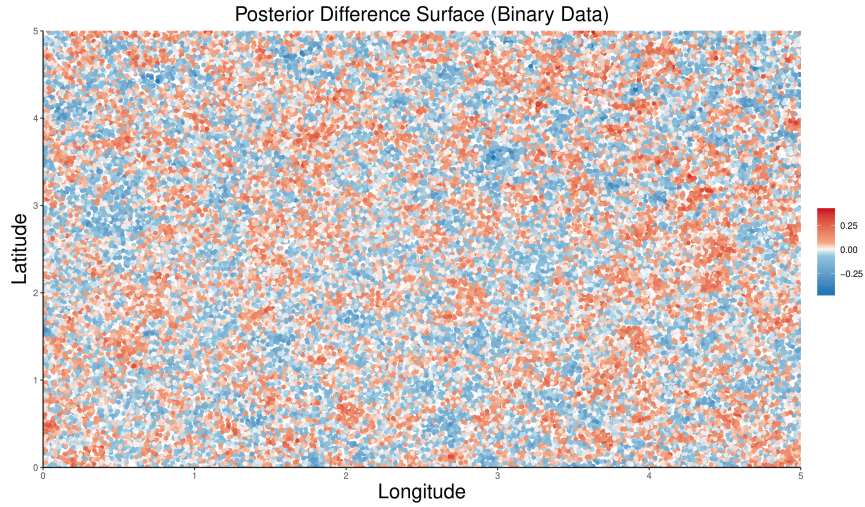


Figure 4: Posterior difference of the probability.

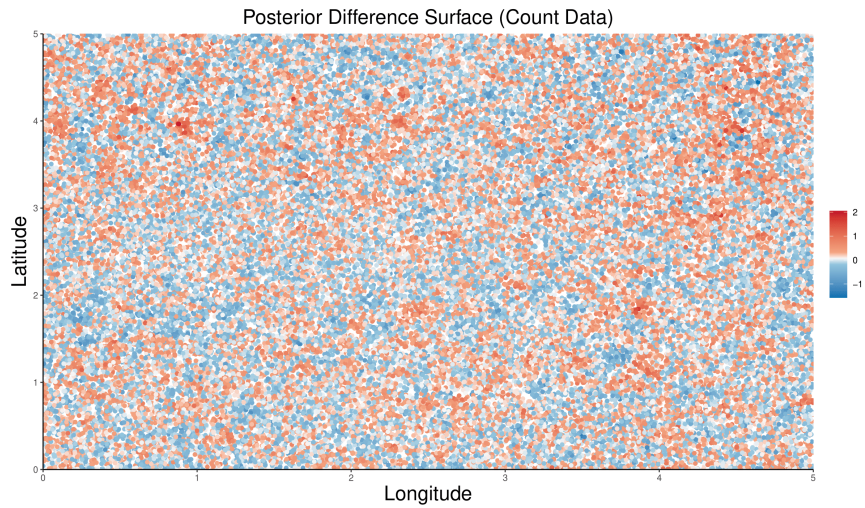


Figure 5: Posterior difference of the log intensity.

9 Coverage Surfaces

Figure 6 below indicates locations where the true probability is not covered by the 95% credible interval. Similarly, Figure 7 indicates locations where the true log intensity is not covered by the 95% credible interval. The respective coverage probabilities are 89.58% and 89.22%, for the binary and count datasets respectively. These are similar to the coverage probabilities from the bisquare basis approach, 88.25% 87.78%.

It is worth noting that regions with higher and lower probabilities in the binary case have smaller coverage probabilities. This is likely due to the lower standard deviations (smaller coverage intervals) associated with higher and lower probabilities. On the other hand, regions with higher log intensities exhibit smaller coverage probabilities, which is interesting. This could potentially be due to the right skewness of the Poisson distribution.

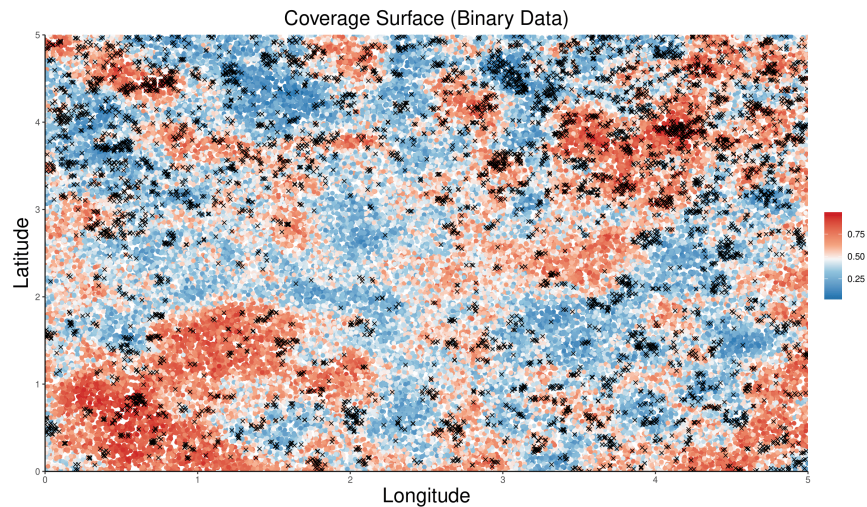


Figure 6: Coverage of Credible Intervals. Each 'x' represents a location where the 95% credible interval does not include the true probability.

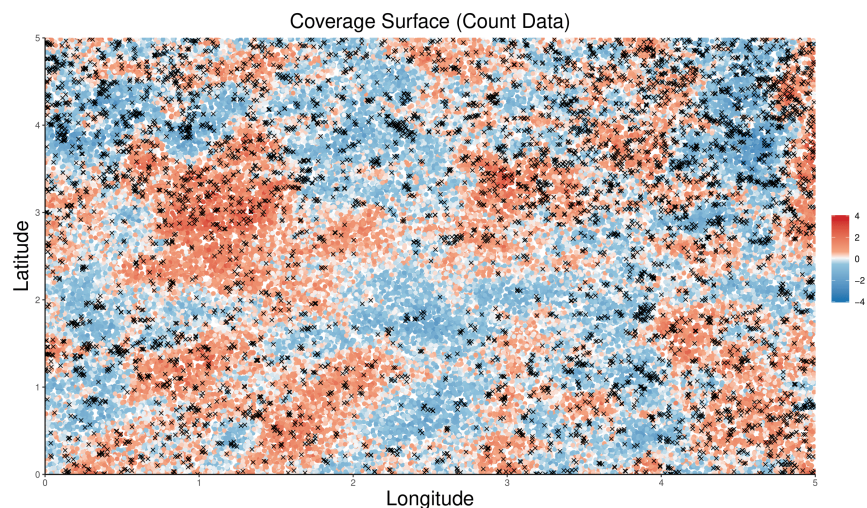


Figure 7: Coverage of Credible Intervals. Each 'x' represents a location where the 95% credible interval does not include the true log intensity.

10 Procedure for choosing K

For practitioners, we suggest searching over a range of possible values. Specifically $K \in \{K_{\min}, \dots, K_{\max}\}$, where $K_{\min} = \max\{4, \lceil \log_{10}(n) \rceil\}$, and K_{\max} is the largest value of K such that each partition contains at least 50 observations. We set the minimum value of K to be at least four because there are four global basis functions with the largest bandwidths. If cross validation is not feasible, one could use Akaike’s information criterion (AIC), the Schwarz-Bayesian criterion (BIC), or adjusted R^2 from a model that includes the covariates, global basis functions, and cluster assignment as predictors. For instance, one can initially cluster observations using $K = \max\{4, \lceil \log_{10}(n) \rceil\}$ clusters and then incrementally increase K either until the decrease in AIC is negligible (using the so-called “elbow” method) or until K_{\max} is reached. An example of this procedure is provided in the supplement. In our simulation study, we compare the performance of our method with various choices of K . In fact, our method is fast enough such that practitioners can explore multiple K settings and ultimately choose the most accurate K based on out-of-sample predictions.

We have implemented an example of this procedure on one nonstationary spatial dataset with 5,000 observations. As displayed in Figure 8, an initial guess for the number of partitions K would be 16 based on the elbow method.

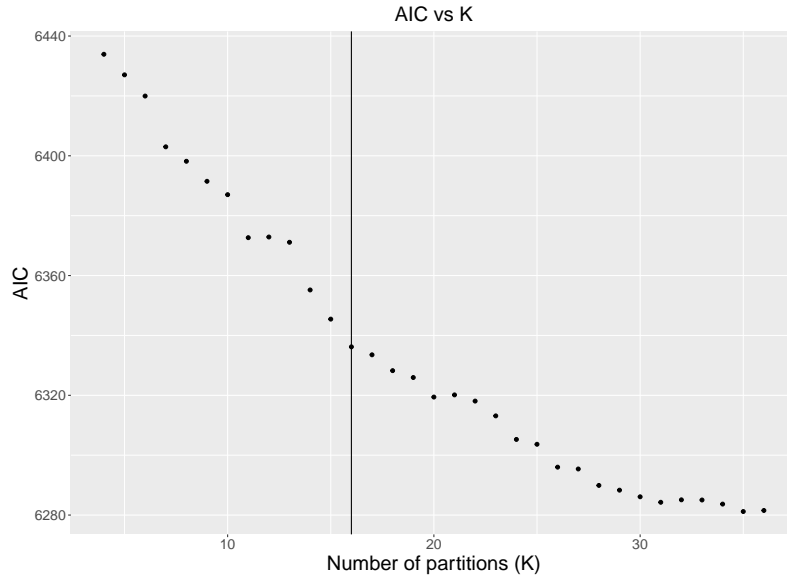


Figure 8: Elbow method for providing an initial estimate for the number of partitions K .

11 Standard Deviation Surfaces for the Real-World Applications

Figure 9 and Figure 10 illustrate the prediction standard deviation surfaces for the Blue Jay abundance and dwarf mistletoe incidence applications, respectively. It can be noted that regions with high predicted intensity exhibit correspondingly high standard deviations for the Blue Jay example. Conversely, regions with both high and low predicted probabilities demonstrate lower standard deviations for the dwarf mistletoe example. These are due to properties of the binomial and Poisson distribution.

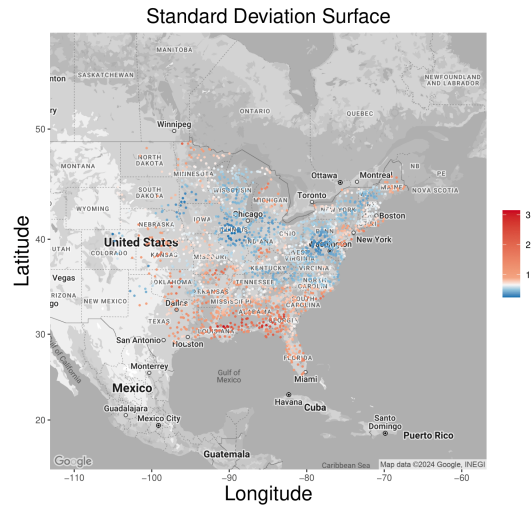


Figure 9: Prediction standard deviation surface for the Blue Jay count data example.

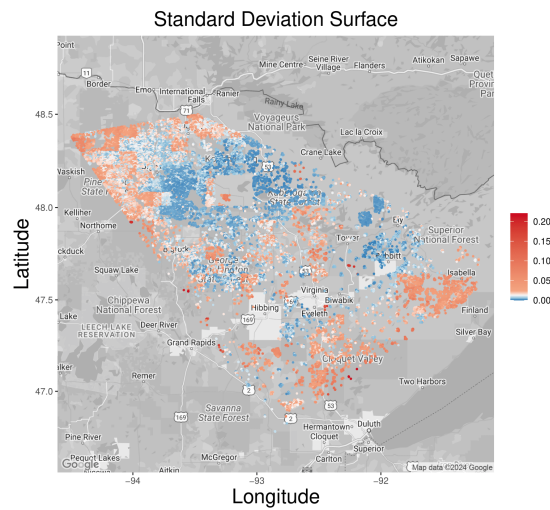


Figure 10: Prediction standard deviation surface for the dwarf mistletoe binary data example.

12 Inference results for the Dwarf Mistletoe Example

Table 2 below displays the parameter estimates for the regression coefficients in the dwarf mistletoe example. Model-fitting results suggest that tree stands with older (higher age) and taller (higher canopy height) dominant trees have a greater probability of dwarf

mistletoe infestation. Conversely, tree stands with a higher basal area per acre and larger stand volume have a lower probability of dwarf mistletoe presence. Each variable is found to be significant, except for basal area, for which the 95% credible interval contains 0.

Covariate	Estimate	95% CI
Age	1.10	(0.76,1.43)
Basal Area	-0.41	(-1.57,0.60)
Height	2.70	(2.42,2.99)
Volume	-1.15	(-1.66,-0.61)

Table 2: Inference results for the mistletoe data. Rows correspond to the predictor variables and columns include the parameter estimates and 95% credible intervals.

References

- Brooks, S. P., Gelman, A., Jones, G. and Meng, X. L. (2011). *Handbook of Markov Chain Monte Carlo*. Chapman and Hall/CRC, Boca Raton.
- Brooks, S. P., Giudici, P. and Roberts, G. O. (2003). Efficient construction of reversible jump Markov chain Monte Carlo proposal distributions. *Journal of the Royal Statistical Society: Series B (Statistical Methodology)* **65(1)**, 3–39.
- Cressie, N. and Johannesson, G. (2008). Fixed rank kriging for very large spatial data sets. *Journal of the Royal Statistical Society: Series B (Statistical Methodology)* **70(1)**, 209–226.
- Denison, D. G. T., Mallick, B. K. and Smith, A. F. M. (1998). Automatic Bayesian curve fitting. *Journal of the Royal Statistical Society: Series B (Statistical Methodology)* **60(2)**, 333–350.
- Fan, Y. and Brooks, S. P. (2000). Bayesian modelling of prehistoric corbelled domes. *Journal of the Royal Statistical Society: Series D (The Statistician)* **49(3)**, 339–354.

- Fuentes, M. (2001). A high frequency kriging approach for non-stationary environmental processes. *Environmetrics* **12(5)**, 469–483.
- Green, P. J. (1995). Reversible jump Markov chain Monte Carlo computation and Bayesian model determination. *Biometrika* **82(4)**, 711–732.
- Heaton, M. J., Christensen, W. F. and Terres, M. A. (2017). Nonstationary Gaussian process models using spatial hierarchical clustering from finite differences. *Technometrics* **59(1)**, 93–101.
- Nott, D. J. and Dunsmuir, W. T. (2002). Estimation of nonstationary spatial covariance structure. *Biometrika* **89(4)**, 819–829.
- Nott, D. J. and Leonte, D. (2004). Sampling schemes for Bayesian variable selection in generalized linear models. *Journal of Computational and Graphical Statistics* **13(2)**, 362–382.
- Richardson, S. and Green, P. J. (1997). On Bayesian analysis of mixtures with an unknown number of components (with discussion). *Journal of the Royal Statistical Society: Series B (Statistical Methodology)* **59(4)**, 731–792.
- Sengupta, A. and Cressie, N. (2013). Hierarchical statistical modeling of big spatial datasets using the exponential family of distributions. *Spatial Statistics* **4**, 14–44.